NASA TECHNICAL NOTE

NASA TN D-3755

NASA TN D-3755



# EFFECTS OF CONFIGURATION GEOMETRY ON THE SUPERSONIC AERODYNAMIC CHARACTERISTICS OF A SIMULATED LAUNCH VEHICLE

*by Richard D. Samuels and James A. Blackwell, Jr.*

*Langley Research Center*
*Langley Station, Hampton, Va.*

NATIONAL AERONAUTICS AND SPACE ADMINISTRATION • WASHINGTON, D. C. • JANUARY 1967

NASA TN D-3755

# EFFECTS OF CONFIGURATION GEOMETRY ON THE SUPERSONIC AERODYNAMIC CHARACTERISTICS OF A SIMULATED LAUNCH VEHICLE

By Richard D. Samuels and James A. Blackwell, Jr.

Langley Research Center
Langley Station, Hampton, Va.

NATIONAL AERONAUTICS AND SPACE ADMINISTRATION

For sale by the Clearinghouse for Federal Scientific and Technical Information
Springfield, Virginia 22151 – Price $2.00

# EFFECTS OF CONFIGURATION GEOMETRY ON THE SUPERSONIC AERODYNAMIC CHARACTERISTICS OF A SIMULATED LAUNCH VEHICLE

By Richard D. Samuels and James A. Blackwell, Jr.
Langley Research Center

## SUMMARY

An investigation to determine the effects of nose-cone angle, upper-stage fineness ratio, and transition-flare angle on the aerodynamic force and moment characteristics of a simulated launch vehicle was conducted at Mach numbers from 1.60 to 2.86, angles of attack from $-4^{\circ}$ to $10^{\circ}$, and a Reynolds number of $2 \times 10^6$ per foot ($6.56 \times 10^6$ per meter). The results of this investigation are compared with values calculated from empirical and theoretical methods presented in NASA TN D-3283, NACA Report 1328, and NACA TN 3391.

The results indicate that increasing the nose-cone half-angle from $15.3^{\circ}$ to $30^{\circ}$ has no appreciable effect on normal-force, pitching-moment, or center-of-pressure characteristics. However, this increase in nose-cone angle roughly doubled the axial force.

An increase in the upper-stage fineness ratio from 1.42 to 4.85 causes an increase in axial force along with an increase in pitching-moment coefficient and a forward movement of the center-of-pressure location. The normal-force coefficients are unaffected by variations in upper-stage fineness ratio.

Increasing the transition-flare angle tends to increase the axial force while having no noticeable effect on the other aerodynamic force and moment characteristics.

## INTRODUCTION

A series of investigations (refs. 1 to 5) has been conducted at the NASA Langley Research Center to determine the effects of configuration geometry on the transonic and supersonic aerodynamic characteristics of simulated two-stage launch vehicles. The transonic aerodynamic force and moment results are reported in references 2 and 4 and the transonic aerodynamic-pressure and section normal-force-coefficient distributions are presented in references 1 and 3.

As an adjunct to the supersonic aerodynamic-loads investigation of reference 5, the present investigation was undertaken to determine the effect of variations in nose-cone

angle, upper-stage fineness ratio, and stage-transition-flare angle on the supersonic aerodynamic force and moment characteristics of two-stage simulated launch vehicles.

The aerodynamic force and moment results of the investigation are compared with those computed from the methods described in references 6, 7, and 8.

The investigation was conducted in the Langley Unitary Plan wind tunnel over a Mach number range from 1.60 to 2.86. The Reynolds number of the investigation was $2.0 \times 10^6$ per foot ($6.56 \times 10^6$ per meter). The angle of attack varied generally from $-4^\circ$ to $10^\circ$.

## SYMBOLS

The units for the physical quantities used in this paper are given in both U.S. Customary Units and in the International System of Units (SI). The physical quantities given in SI Units are given in parentheses. Factors relating the two systems are given in reference 9.

Aerodynamic force and moment data are referred to the body system of axes, with coefficients based on the maximum body cross-sectional area of 0.0524 foot$^2$ (0.0048 meter$^2$) and the maximum body diameter of 3.10 inches (7.87 cm). The area over which the base pressure was assumed to be acting was taken to be 0.0357 foot$^2$ (0.0033 meter$^2$), and the area acted on by the chamber pressure was taken to be 0.0167 foot$^2$ (0.0015 meter$^2$). Moments are measured about a point located on the body center line, 3 reference diameters forward of the model base.

$C_A$ axial-force coefficient, $\frac{\text{Axial force}}{qA}$

$C_{A,b}$ base axial-force coefficient, $\frac{\text{Base axial force}}{qA}$

$C_{A,c}$ chamber axial-force coefficient, $\frac{\text{Chamber axial force}}{qA}$

$C_m$ pitching-moment coefficient, $\frac{\text{Pitching moment}}{qAd}$

$C_{m_\alpha}$ pitching-moment-curve slope, $\frac{\partial C_m}{\partial \alpha}$, per degree

$C_N$ normal-force coefficient, $\frac{\text{Normal force}}{qA}$

$C_{N_\alpha}$ normal-force-curve slope, $\frac{\partial C_N}{\partial \alpha}$, per degree

| | |
|---|---|
| $A$ | maximum body cross-sectional area, feet$^2$ (meters$^2$) |
| $d$ | maximum body diameter, inches (centimeters) |
| $M$ | Mach number |
| $q$ | free-stream dynamic pressure, pounds/foot$^2$ (newtons/meter$^2$) |
| $x_{cp}$ | center-of-pressure location, maximum body diameters forward of model base |
| $\alpha$ | angle of attack of body center line, degrees |
| $\delta_F$ | stage-transition flare half-angle, degrees |
| $\delta_N$ | nose-cone half-angle, degrees |

## APPARATUS AND MODEL

### Apparatus

The investigation was conducted in the low supersonic speed test section of the Langley Unitary Plan wind tunnel. The test section is 4 feet (1.22 m) square and approximately 7 feet (2.13 m) in length. The nozzle leading to the test section is of the asymmetric sliding block type which allows the Mach number to be varied continuously through a range from 1.5 to 2.86. Further details of the wind tunnel may be found in reference 10.

Force and moment measurements were made through the use of a six-component internal strain-gage balance. The model was mounted in the wind tunnel on a remote-controlled center-line sting. Balance-chamber pressure and model-base pressure were measured by means of static orifices located in the balance cavity and at the model base, respectively.

### Model

Figure 1 shows the details and dimensions of the various configurations tested. The configurations are identical to those of references 1, 2, 3, and 5 and are numbered to conform to the numbering system of reference 1. It should be noted that the configuration numbers do not follow an orderly progression as far as geometric progressions are concerned.

Nose-angle variations.- Configurations used to determine effects of nose half-angle (fig. 1(a)) had an upper-stage fineness ratio of 4.85, and a transition-flare half-angle of 5°.

Three pointed nose cones (configurations 3, 4, and 5) having half-angles of $15.3^{\circ}$, $22.5^{\circ}$, and $30^{\circ}$ were investigated.

Upper-stage fineness-ratio variations.- The configurations shown in figure 1(b) were used to determine the effects of fineness ratio. The nose-cone and transition-flare half-angles were $22.5^{\circ}$ and $5^{\circ}$, respectively; the fineness ratios were 1.42, 2.99, and 4.85 for configurations 1, 2, and 3, respectively.

Transition-flare-angle variations.- Four configurations (3, 10, 8, and 9) were used to study the effects of variations in stage-transition-flare angle. Each configuration had a nose-cone half-angle of $22.5^{\circ}$ and the transition-flare half-angles were $5^{\circ}$, $10^{\circ}$, $15^{\circ}$, and $29.9^{\circ}$. (See fig. 1(c).) The variation in transition-flare angle was accompanied by varying the upper-stage fineness ratio and overall length in the same manner described in reference 1. These variations, which in reference 1 resulted from an attempt to place pressure orifices immediately ahead of the flare leading edge, were duplicated for the configurations of the present investigation.

## Tests and Procedures

The investigation was conducted at a Reynolds number of $2.0 \times 10^6$ per foot ($6.56 \times 10^6$ per meter) and a total temperature of approximately $610^{\circ}$ R ($338^{\circ}$ K). The Mach number range was from 1.60 to 2.86 and the angle-of-attack range extended generally from $-4^{\circ}$ to $10^{\circ}$.

The investigation was conducted with a boundary-layer transition strip 0.1 inch (0.254 cm) wide located at the nose-cone upper-stage juncture. The transition strip consisted of No. 60 carborundum grains, with a nominal diameter = 0.0117 in. (0.0297 cm), set in a plastic adhesive.

# CORRECTIONS AND ACCURACY

## Corrections

The angles of attack of the model have been corrected for deflection of the balance and sting under load and for tunnel-flow angularity. Axial-force results contained herein have been adjusted to the assumed condition of free-stream static pressure acting at the model base and in the balance chamber.

## Accuracy

Based upon instrument calibrations, it is estimated that the various measured quantities are generally accurate within the following limits:

| | |
|---|---|
| $C_N$ | ±0.020 |
| $C_A$ | ±0.010 |
| $C_{A,b}$ | ±0.005 |
| $C_{A,c}$ | ±0.005 |
| $C_m$ | ±0.04 |
| $\alpha$, deg | ±0.10 |
| M | ±0.015 |

## PRESENTATION OF RESULTS

The results of this investigation are presented in the figures listed in the following table:

| | Figure |
|---|---|
| Variation with angle of attack of normal-force characteristics | 2 |
| Variation with angle of attack of axial-force characteristics | 3 |
| Variation with angle of attack of base axial-force characteristics | 4 |
| Variation with angle of attack of chamber axial-force characteristics | 5 |
| Variation with angle of attack of pitching-moment characteristics | 6 |
| Variation with angle of attack of center-of-pressure characteristics | 7 |
| Summary of aerodynamic characteristics in pitch, $\alpha = 0^o$ | 8 |

Flagged points which appear in the center-of-pressure results in figure 7 represent values obtained by using $C_{m_\alpha}$ and $C_{N_\alpha}$ measured through $0^o$ angle of attack. Presented in figure 8 are the empirical predictions of the aerodynamic characteristics as obtained from references 6, 7, and 8.

## RESULTS AND DISCUSSION

### Effect of Nose-Cone Angle

The variation of normal-force coefficient with angle of attack for various nose-cone angles is shown in figure 2(a). The effect of nose-cone-angle variation is seen to be slight at all Mach numbers. The slopes of the normal-force curves, however, increase at angles of attack greater than about $4^o$ for all configurations. Figure 8(a) indicates that at $\alpha = 0^o$ there is no measurable effect of nose-cone-angle variation on the slope of the normal-force curve over the entire range of Mach numbers. The empirical normal-force-curve slopes, presented in figure 8 and computed from reference 6, are

slightly higher than the measured values and also show no variation with nose-cone half-angle.

Figure 3(a) shows there is a large effect of nose-cone angle on the axial-force coefficients. For $\delta_N = 30^\circ$, the axial-force coefficient is approximately twice that for $\delta_N = 15.3^\circ$. The results of this investigation also indicate that the axial-force coefficients measured are essentially independent of angle of attack through the range of this investigation. The axial-force coefficients decrease with increasing Mach number as shown in figure 8(a). Also shown in figure 8(a) is the axial force as predicted from second-order shock expansion theory (ref. 7) along with the empirical skin-friction theory of reference 8. The wave drag was obtained from reference 7 and added to the skin-friction drag obtained from reference 8. The prediction of both the effect of Mach number and nose-cone angle is accurate. Figures 4(a) and 5(a) show no effect of nose-cone-angle variation on either the base or chamber axial-force coefficients. There is, however, a slight increase in these coefficients with increasing angle of attack.

Effects of a variation in nose-cone angle on the moment coefficients and center-of-pressure characteristics, shown in figures 6(a) and 7(a) and summarized in figure 8(a), are seen to be slight.

### Effect of Upper-Stage Fineness Ratio

No significant effect of upper-stage fineness ratio on the normal-force coefficients is evident from figure 2(b).

The empirical results presented in figure 8(b) as computed from reference 6 generally show slight variations of normal-force-curve slope and center of pressure with fineness ratio. The slope of the normal-force curve increases with increasing angle of attack; however, as shown in figure 8(b), there is no appreciable variation of either the measured or the calculated normal-force-curve slopes through $\alpha = 0^\circ$ with Mach number.

Figure 3(b) shows an increase in axial-force coefficient with increase in upper-stage fineness ratio. This increase, which remains essentially constant over the entire angle-of-attack range, is probably due to the increase in skin-friction drag. Figure 8(b) indicates a slight decrease in axial-force coefficient with increasing Mach number. The predicted values again agree well with the measured values. Figures 4(b) and 5(b) show no effect of upper-stage fineness ratio on the base or chamber axial-force coefficients.

There is a notable increase in pitching-moment coefficient with increase in upper-stage fineness ratio as shown in figure 6(b). This increase is to be expected since the nose cone moves farther forward with respect to the moment-reference center. In the summary plot (fig. 8(b)) for $\alpha = 0^\circ$, there are only slight effects in the pitching-moment-curve slope with increasing Mach number. In general, the empirically calculated values

predict the pitching-moment-curve-slope level; however, the measured values do not show the effect of fineness-ratio variation which the empirical method predicts.

Figure 7(b) shows that the center of pressure moves forward with increasing fineness ratio, as would be expected. Figure 8(b) shows the center-of-pressure location to be fairly constant over the Mach number range. This same trend is evident for the empirically calculated values; however, the predicted center-of-pressure location is more rearward than measured location.

### Effect of Transition-Flare Angle

As discussed previously, variations of transition-flare angle were accompanied by variations in the upper-stage fineness ratio. This fact must be considered when comparing the results for varying the transition-flare angle. Figure 2(c) shows no effect of variation in transition-flare angle on the normal-force coefficient. Figure 8(c) shows essentially no change in normal-force-curve slope with Mach number near $\alpha = 0^{\circ}$. The calculated values are in good agreement with the measured values.

Figure 3(c) shows the effect on axial-force coefficient of varying the transition-flare half-angle from $5^{\circ}$ to $29.9^{\circ}$. Some increase would be expected since the fineness ratio has been increased; however, the increase measured during these tests was much greater than that which would be expected as a result of changes in upper-stage fineness ratio. For the configuration with $\delta_F = 29.9^{\circ}$ it is evident that, as the angle of attack is increased from about $3^{\circ}$ to $10^{\circ}$, an increase in axial force occurs. It is believed these variations are probably a result of increasing the angle of attack which causes a decrease in flare-induced separation over the lower portion of the body forward of the flare. This decrease results in sizable increases in positive pressure over the lower half of the flare as the angle of attack is increased. (See ref. 5.)

Figure 8(c) shows that the predicted values agree reasonably well with the measured values for the three lower flare angles. However, because of the detachment of the shock at the flare, no second-order shock-expansion solutions could be obtained for $\delta_F = 29.9^{\circ}$. The measured axial force decreases, as expected, with increasing Mach number. Figures 4(c) and 5(c) show no effect of transition-flare angle on either base or chamber axial-force characteristics.

Figures 6(c) and 7(c) show no effect of transition-flare angle on either the pitching-moment coefficient or the center-of-pressure location. The summary plot (fig. 8(c)) indicates the pitching-moment-curve slope and center-of-pressure location are essentially independent of Mach number. The empirically calculated values are in good agreement with the measured values throughout the Mach number range.

## CONCLUSIONS

Results of an investigation conducted at supersonic speeds to determine the effects of systematic variations in geometry on the aerodynamic characteristics of a simulated launch vehicle have indicated the following:

1. Increasing the nose-cone angle has no appreciable effect on normal-force coefficient, pitching-moment coefficient, or center-of-pressure location. However, increasing the nose-cone angle from $15.3^{\circ}$ to $30^{\circ}$ roughly doubled the axial-force coefficient.

2. An increase in the upper-stage fineness ratio causes an increase in axial-force coefficient along with an increase in pitching moment and a forward movement of the center-of-pressure location. The normal-force coefficients are unaffected by upper-stage fineness-ratio variations.

3. Increasing the transition-flare angle tends to increase the axial-force coefficient but has no noticeable effect on the other force and moment characteristics.

Langley Research Center,
National Aeronautics and Space Administration,
Langley Station, Hampton, Va., September 19, 1966,
124-10-01-01-23.

## REFERENCES


1. Kelly, Thomas C.: Investigation at Transonic Mach Numbers of the Effects of Configuration Geometry on Surface Pressure Distributions For a Simulated Launch Vehicle. NASA TM X-845, 1963.

2. Kelly, Thomas C.; and Ross, Thomas P.: Effects of Configuration Geometry on the Transonic Aerodynamic Characteristics of a Simulated Launch Vehicle. NASA TM X-976, 1964.

3. Kelly, Thomas C.: Aerodynamic Load Distributions at Transonic Speeds for a Group of Simulated Launch-Vehicle Models. NASA TM X-1264, 1966.

4. Langhans, Richard A.; Kelly, Thomas C.; and Hansen, Thomas P.: Effects of Vehicle Geometry on the Transonic Aerodynamic Characteristics of a Simulated Launch Vehicle With Low Upper-Stage Fineness Ratio. NASA TM X-1320, 1966.

5. Blackwell, James A., Jr.: Supersonic Investigation of Effects of Configuration Geometry on Pressure-Coefficient and Section Normal-Force-Coefficient Distributions for a Two-Stage Launch Vehicle. NASA TN D-3408, 1966.

6. Muraca, Ralph J.: An Empirical Method for Determining Static Distributed Aerodynamic Loads on Axisymmetric Multistage Launch Vehicles. NASA TN D-3283, 1966.

7. Syvertson, Clarence A.; and Dennis, David H.: A Second-Order Shock-Expansion Method Applicable to Bodies of Revolution Near Zero Lift. NACA Report 1328, 1957.

8. Sommer, Simon C.; and Short, Barbara J.: Free-Flight Measurements of Turbulent-Boundary-Layer Skin Friction in the Presence of Severe Aerodynamic Heating at Mach Numbers From 2.8 to 7.0. NACA TN 3391, 1955.

9. Mechtly, E. A.: The International System of Units – Physical Constants and Conversion Factors. NASA SP-7012, 1964.

10. Anon.: Manual for Users of the Unitary Plan Wind Tunnel Facilities of the National Advisory Committee for Aeronautics. NACA, 1956.

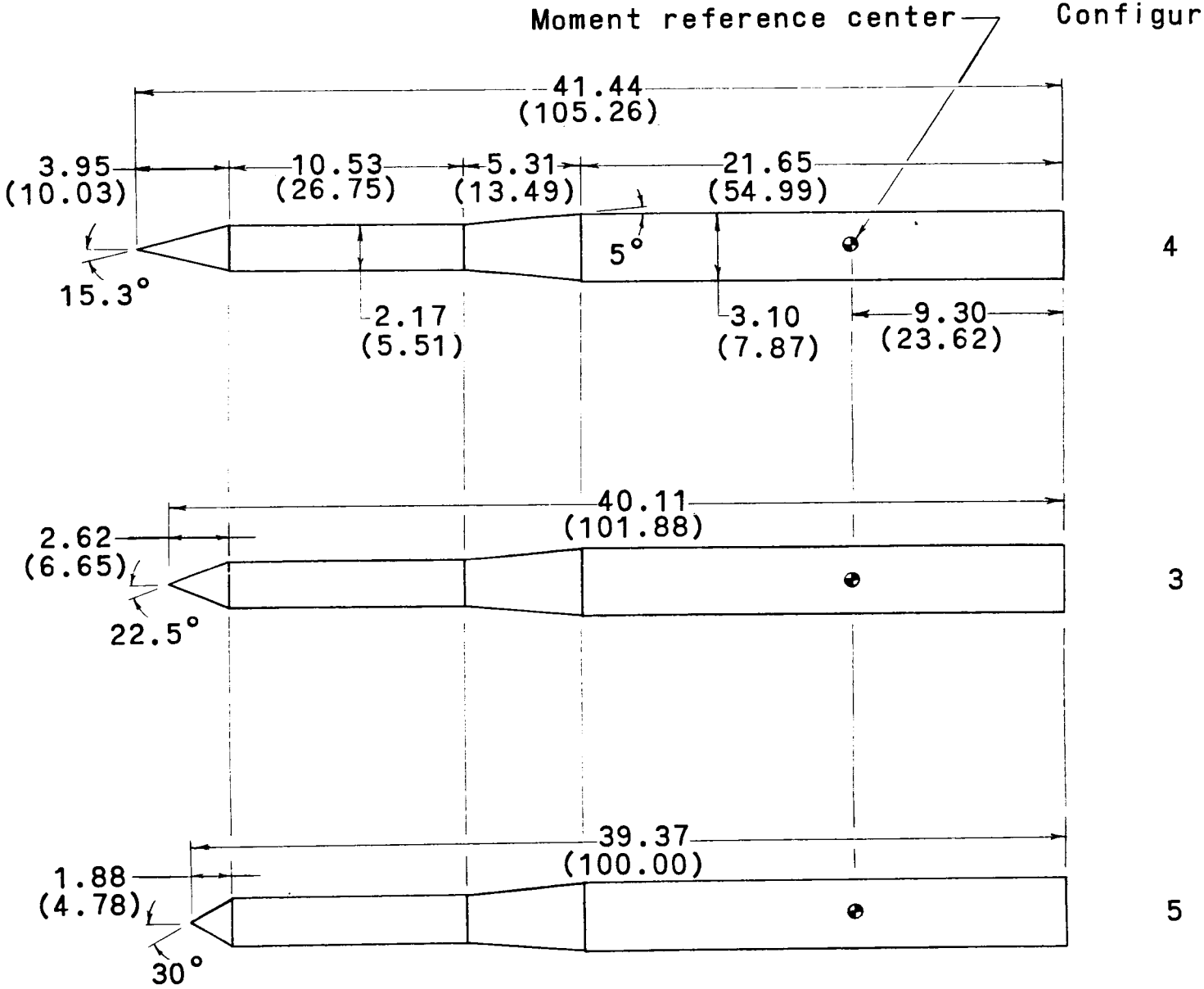


(a) Nose-cone-angle variations.

Figure 1.- Model details. All dimensions in inches unless otherwise noted. (Centimeters in parentheses.)

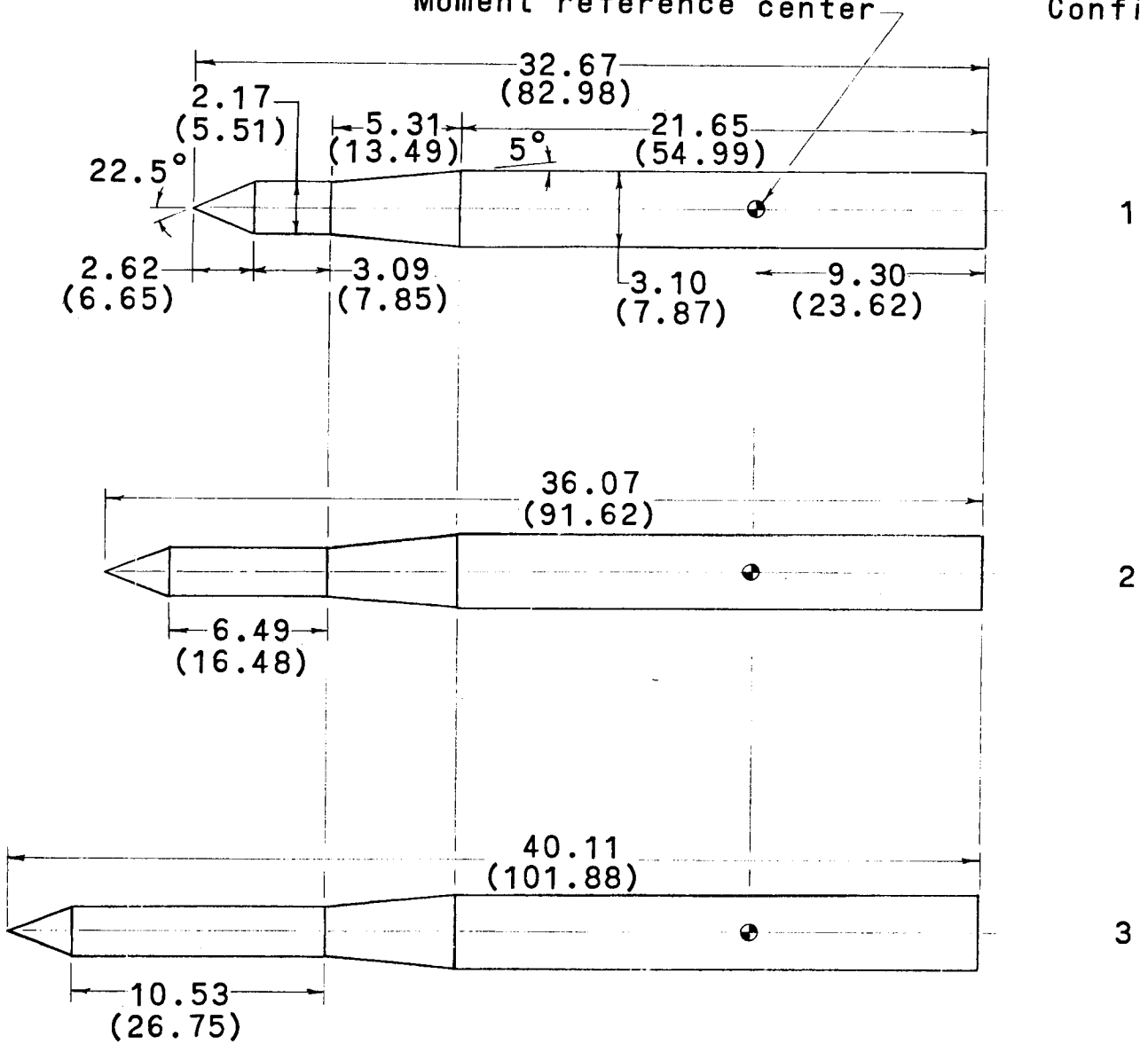


(b) Upper-stage fineness-ratio variations.

Figure 1.- Continued.

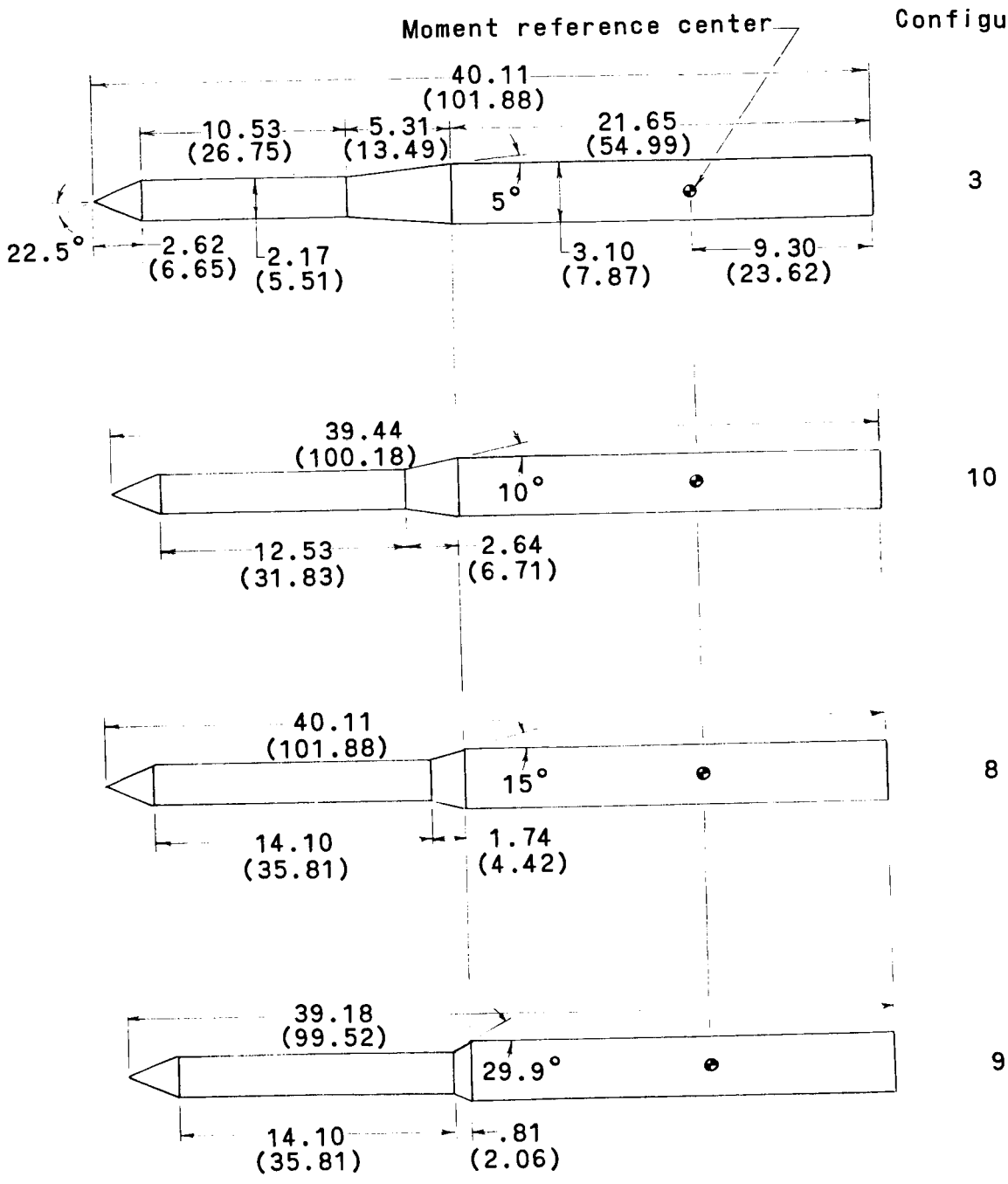


(c) Transition-flare-angle variations.

Figure 1.- Concluded.

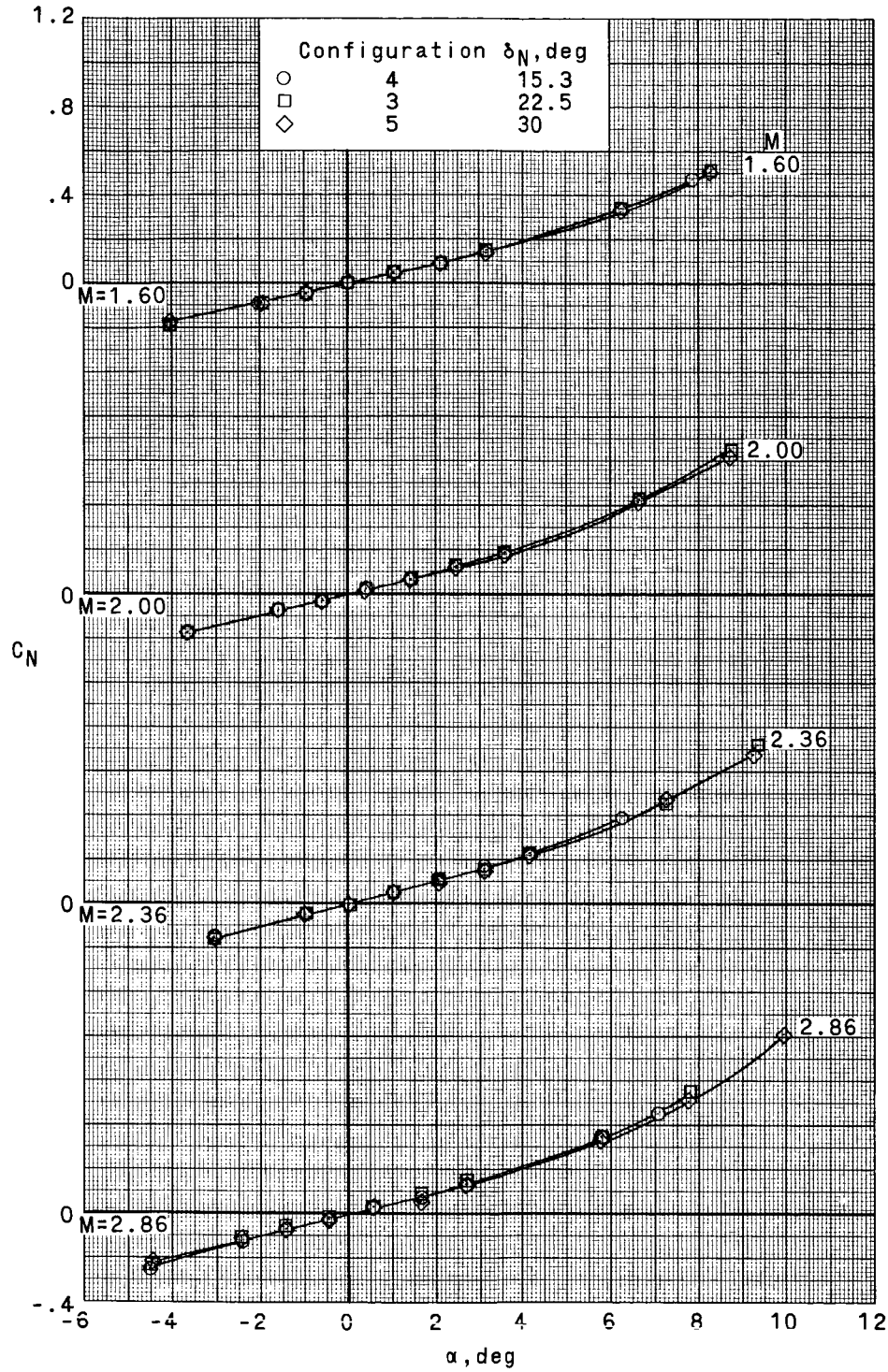


(a) Nose-cone-angle variations.

Figure 2.- Variation with angle of attack of normal-force characteristics.

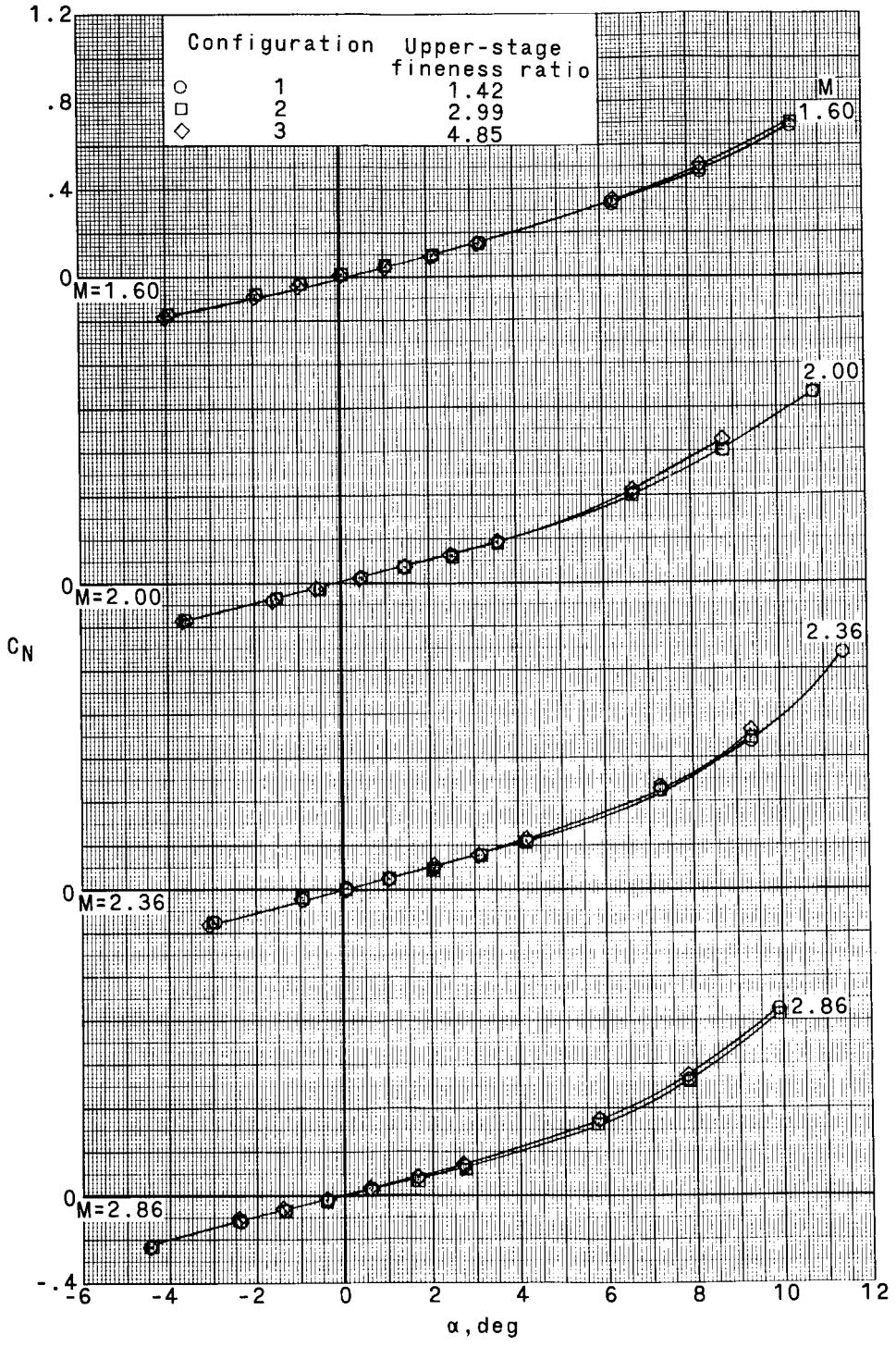


(b) Upper-stage fineness-ratio variations.

Figure 2.- Continued.

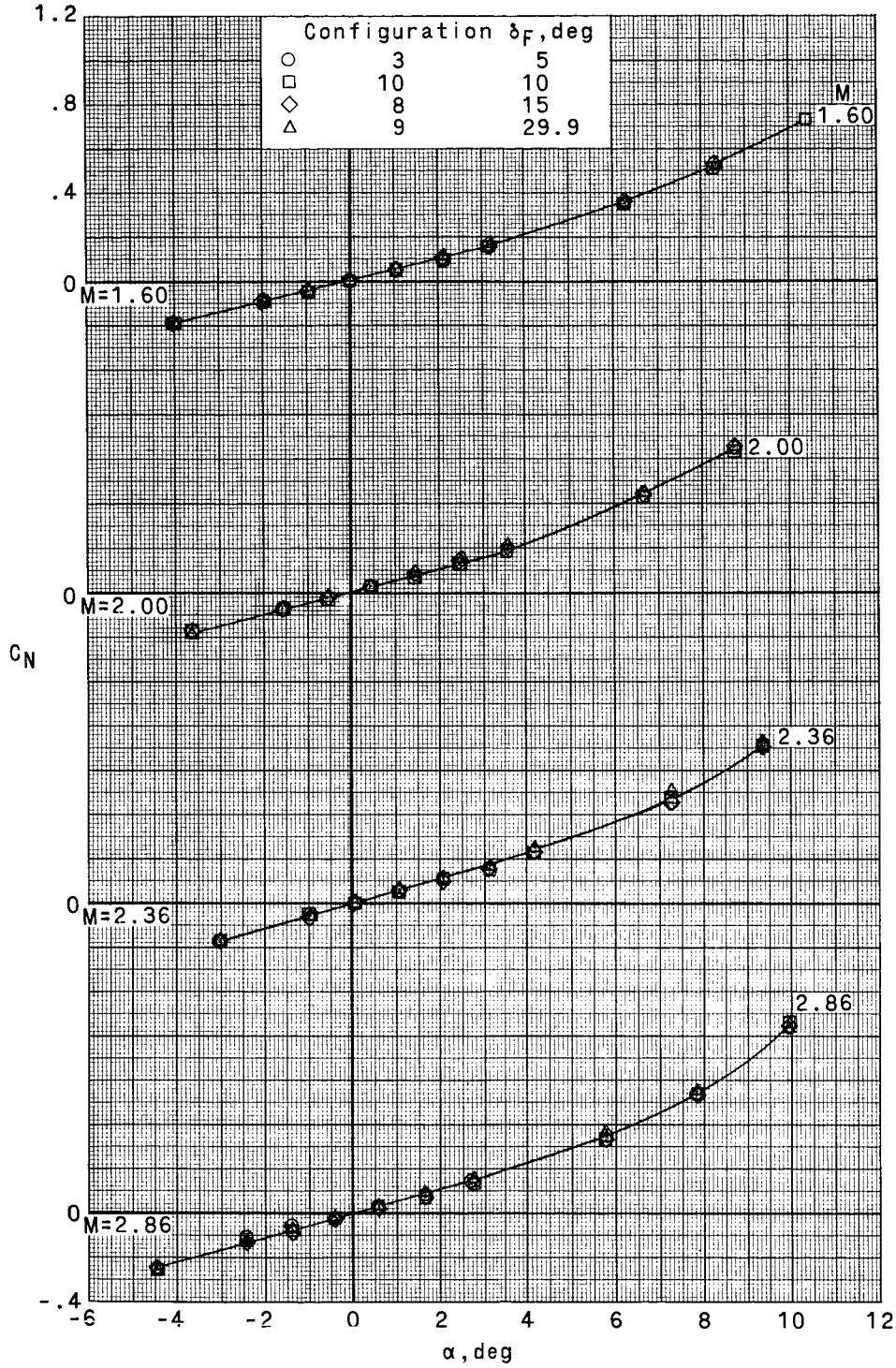


(c) Transition-flare-angle variations.

Figure 2.- Concluded.

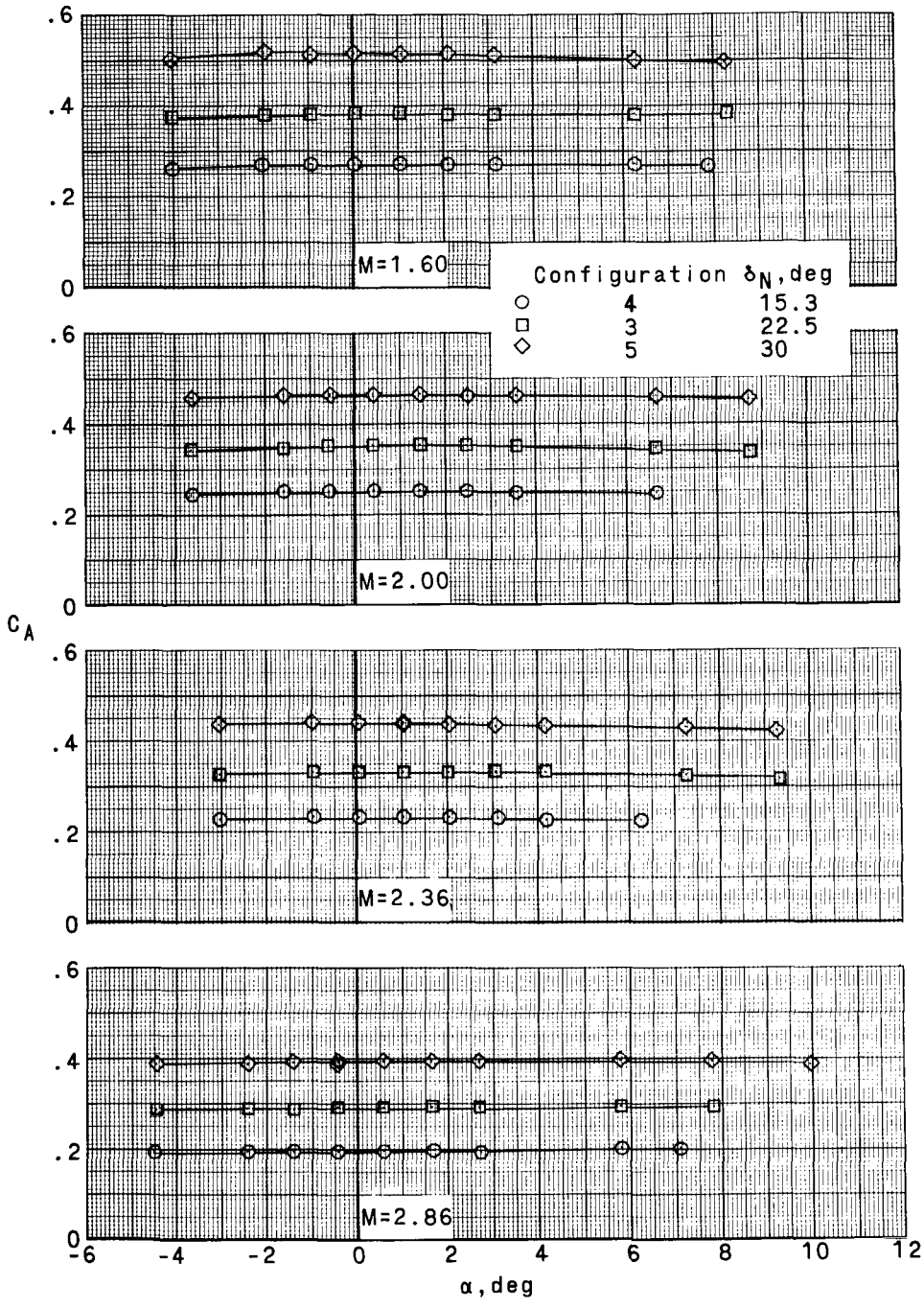


(a) Nose-cone-angle variations.

Figure 3.- Variation with angle of attack of axial-force characteristics.

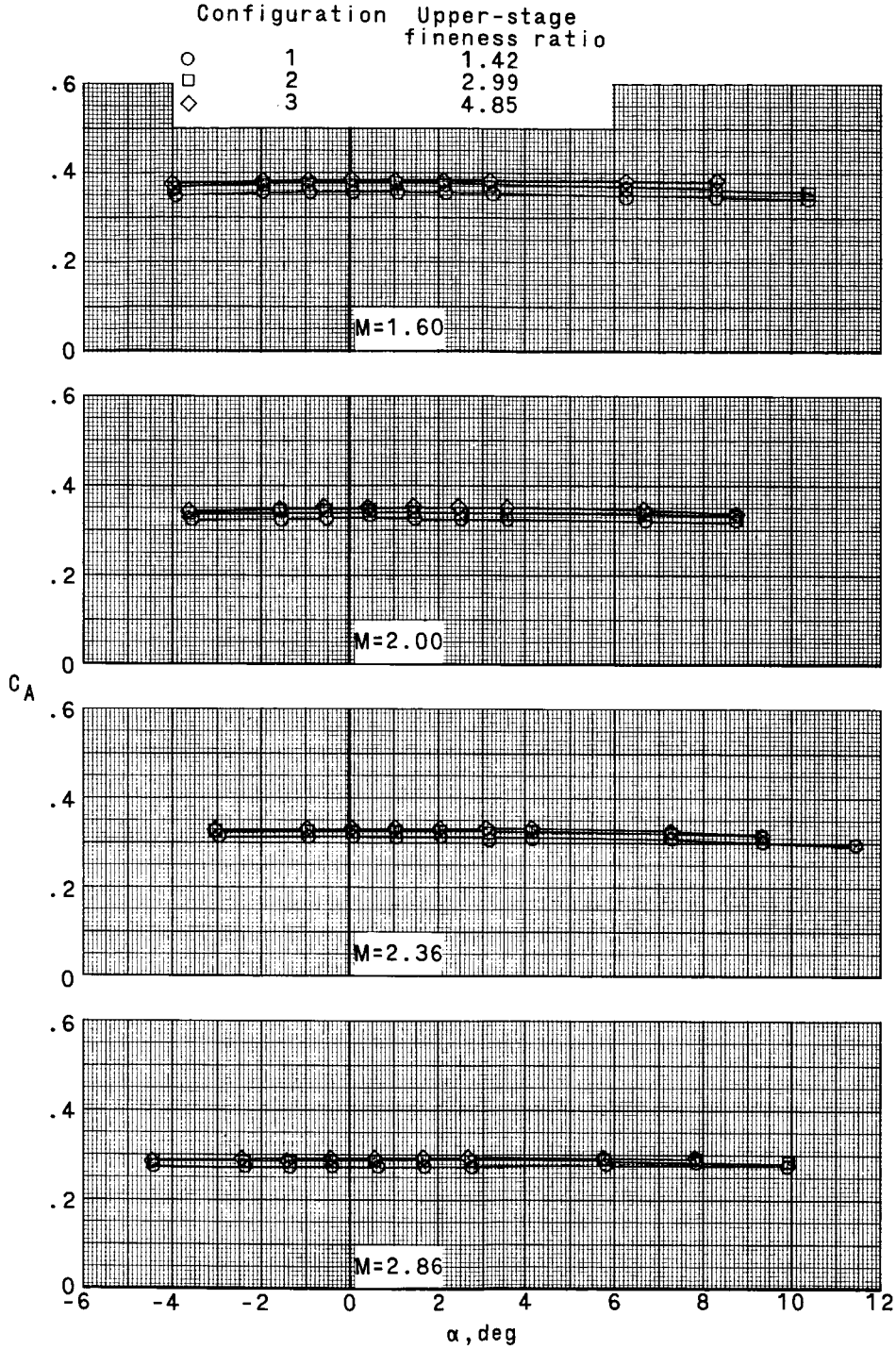


(b) Upper-stage fineness-ratio variations.

Figure 3.- Continued.

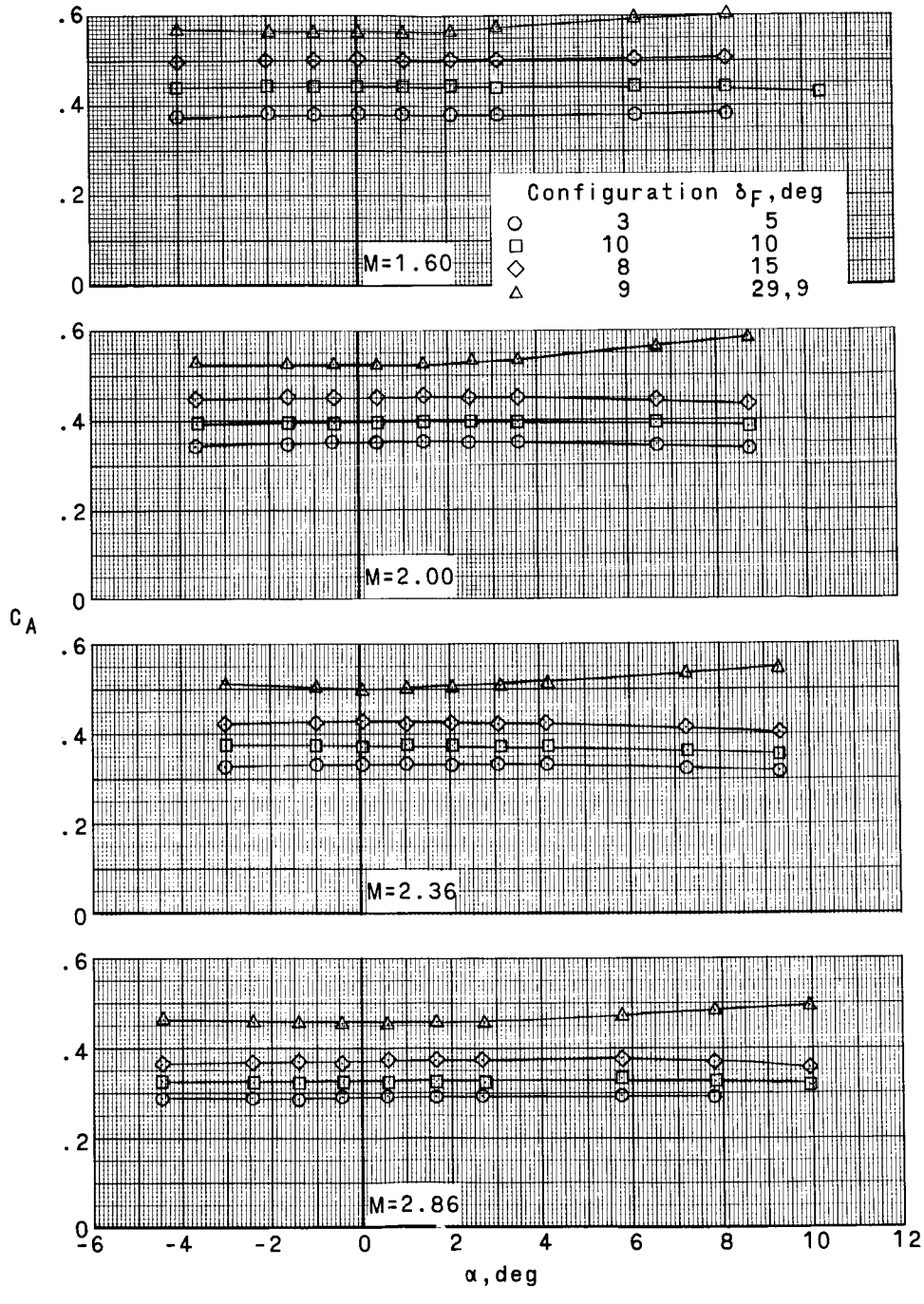


(c) Transition-flare-angle variations.

Figure 3.- Concluded.

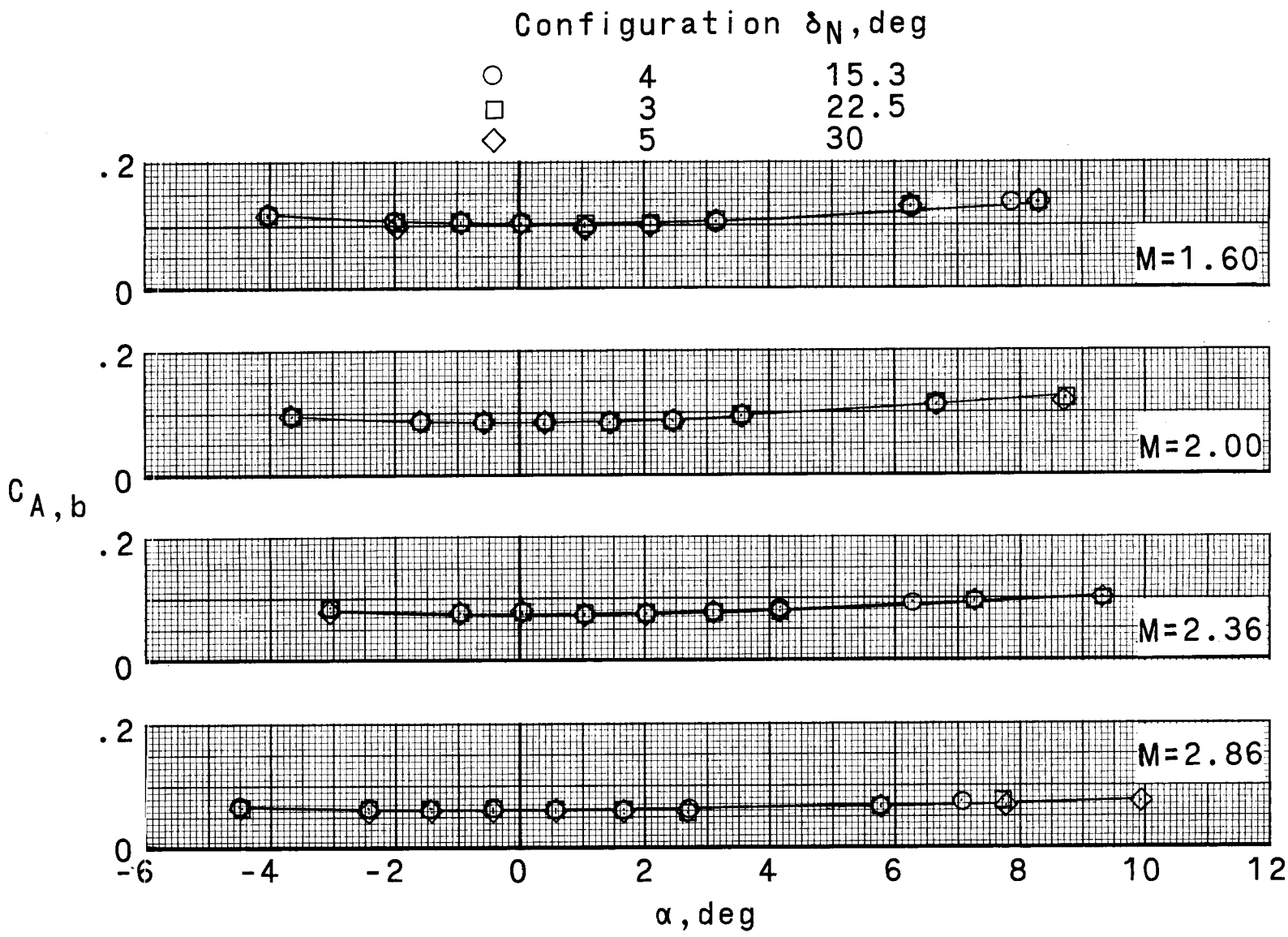


(a) Nose-cone-angle variations.

Figure 4.- Variation with angle of attack of base axial-force characteristics.

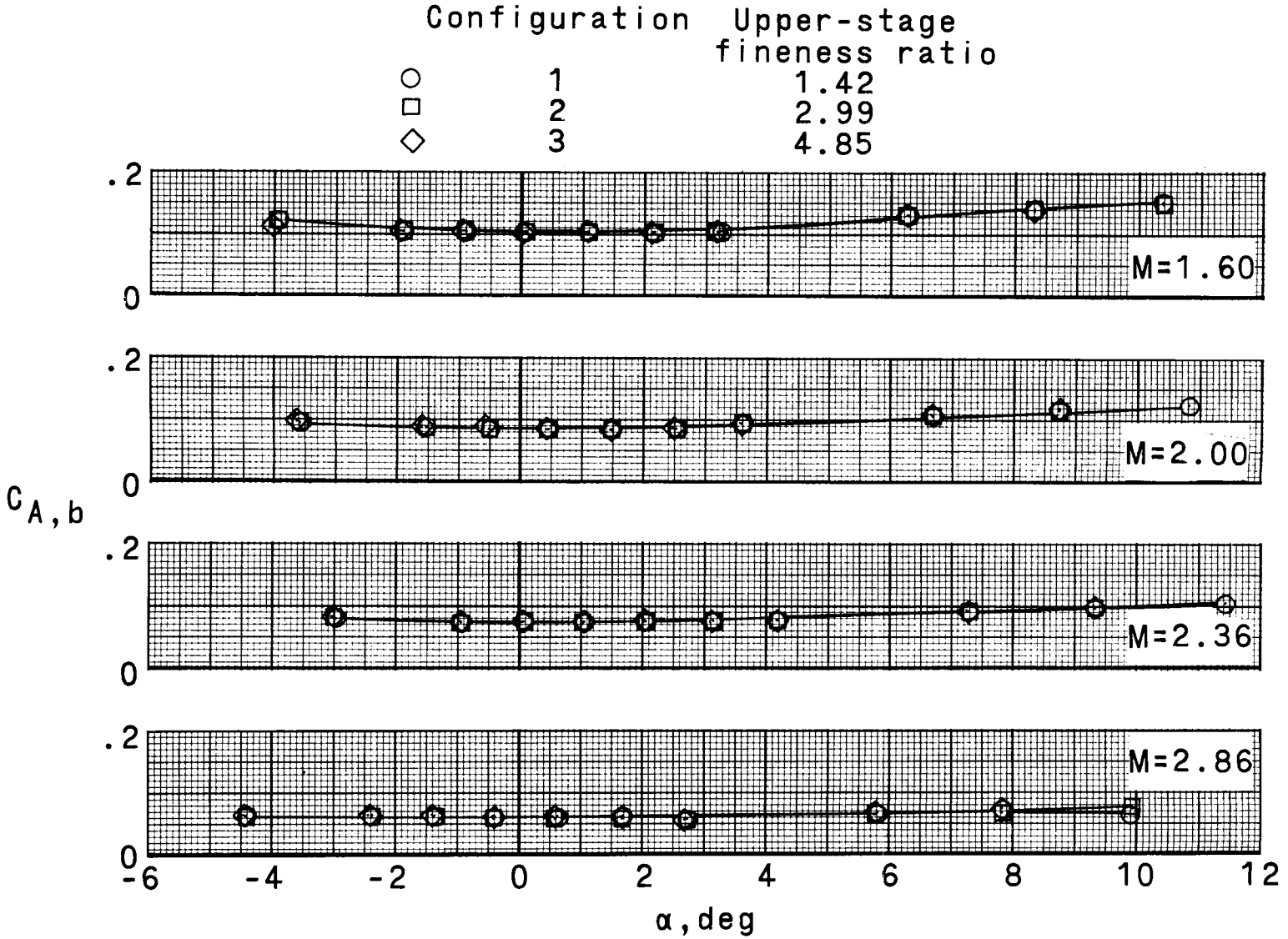


(b) Upper-stage fineness-ratio variations.

Figure 4.- Continued.

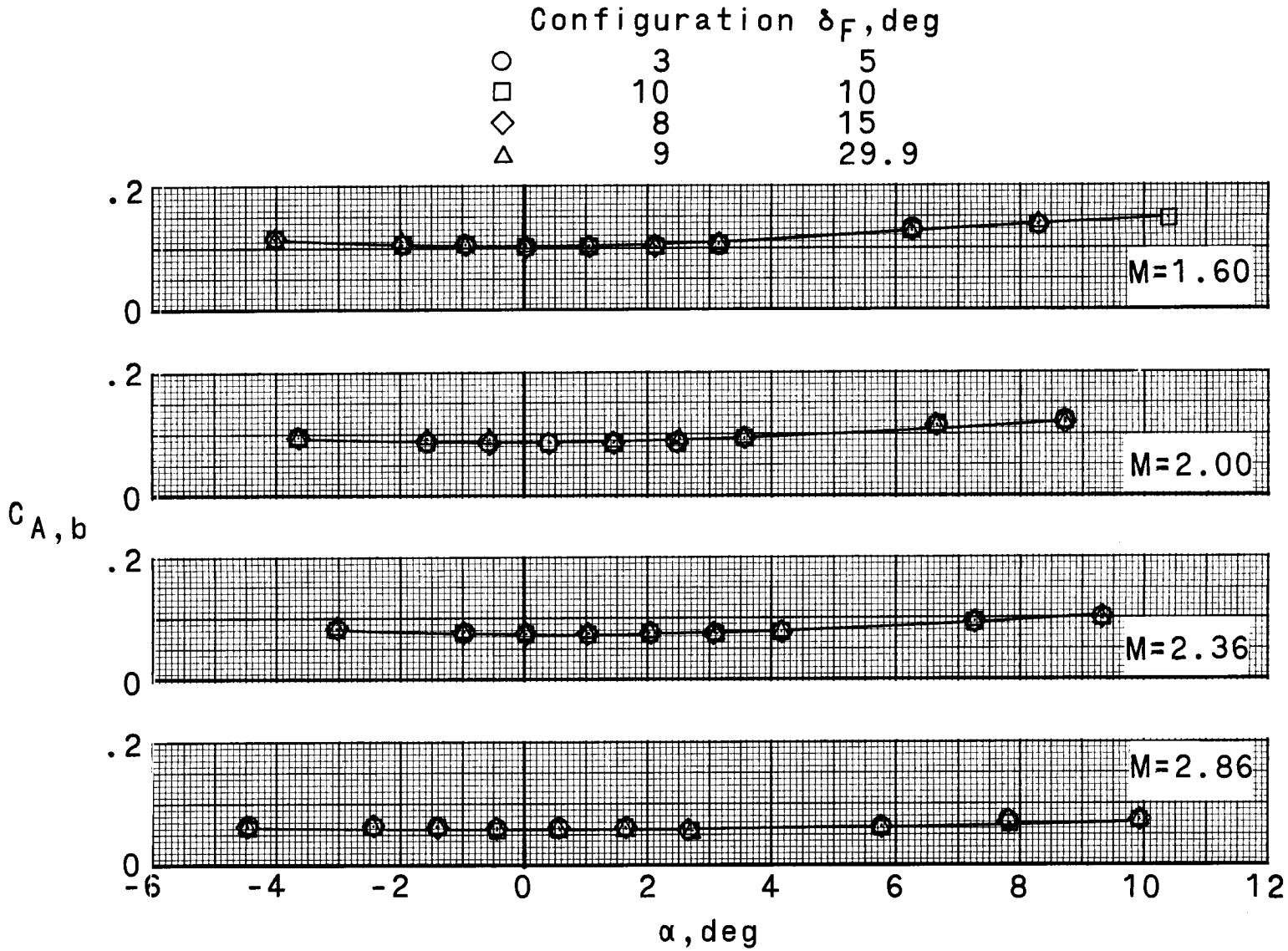


(c) Transition-flare-angle variations.

Figure 4.- Concluded.

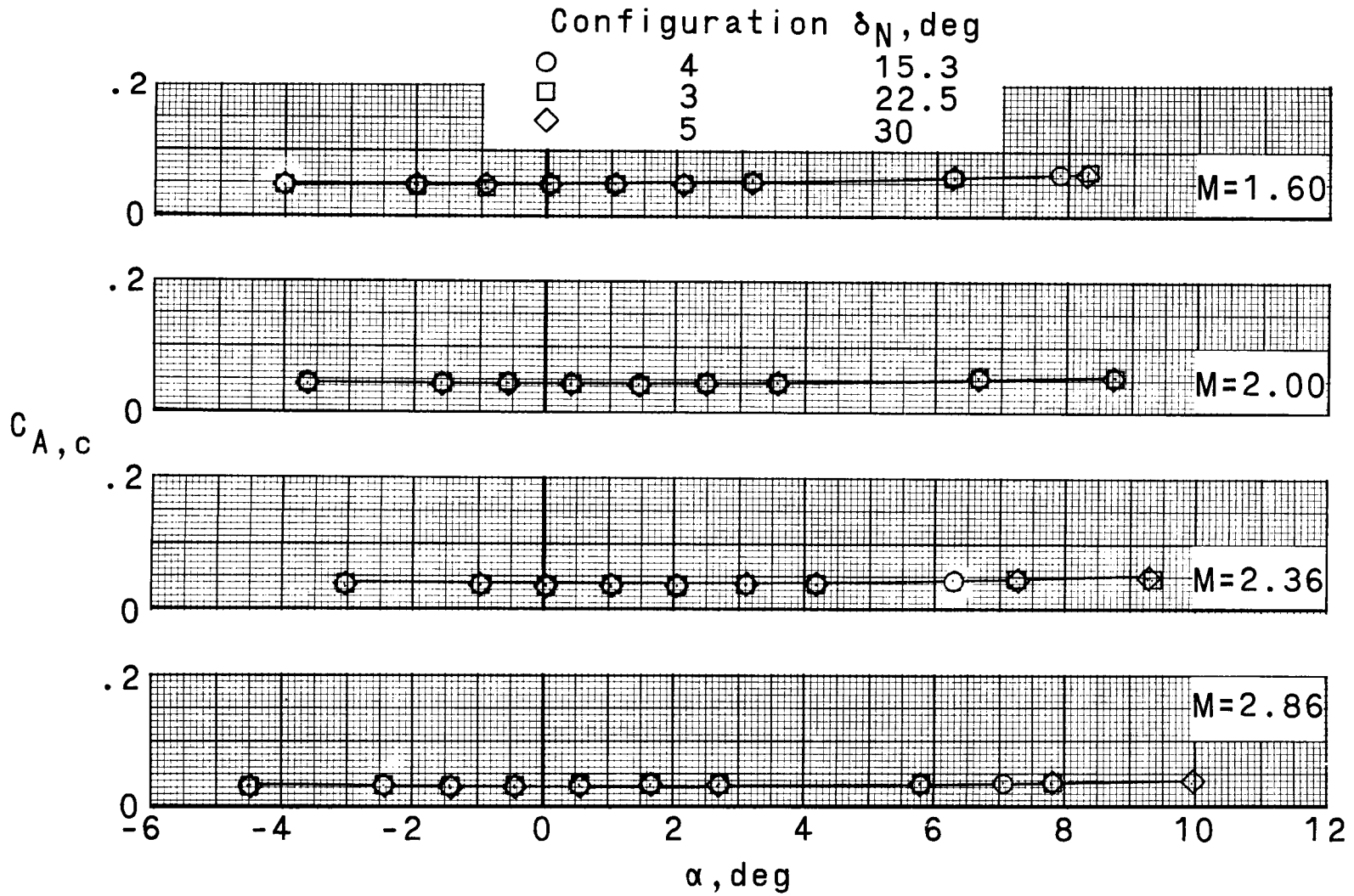


(a) Nose-cone-angle variations.

Figure 5.- Variation with angle of attack of chamber axial-force characteristics.

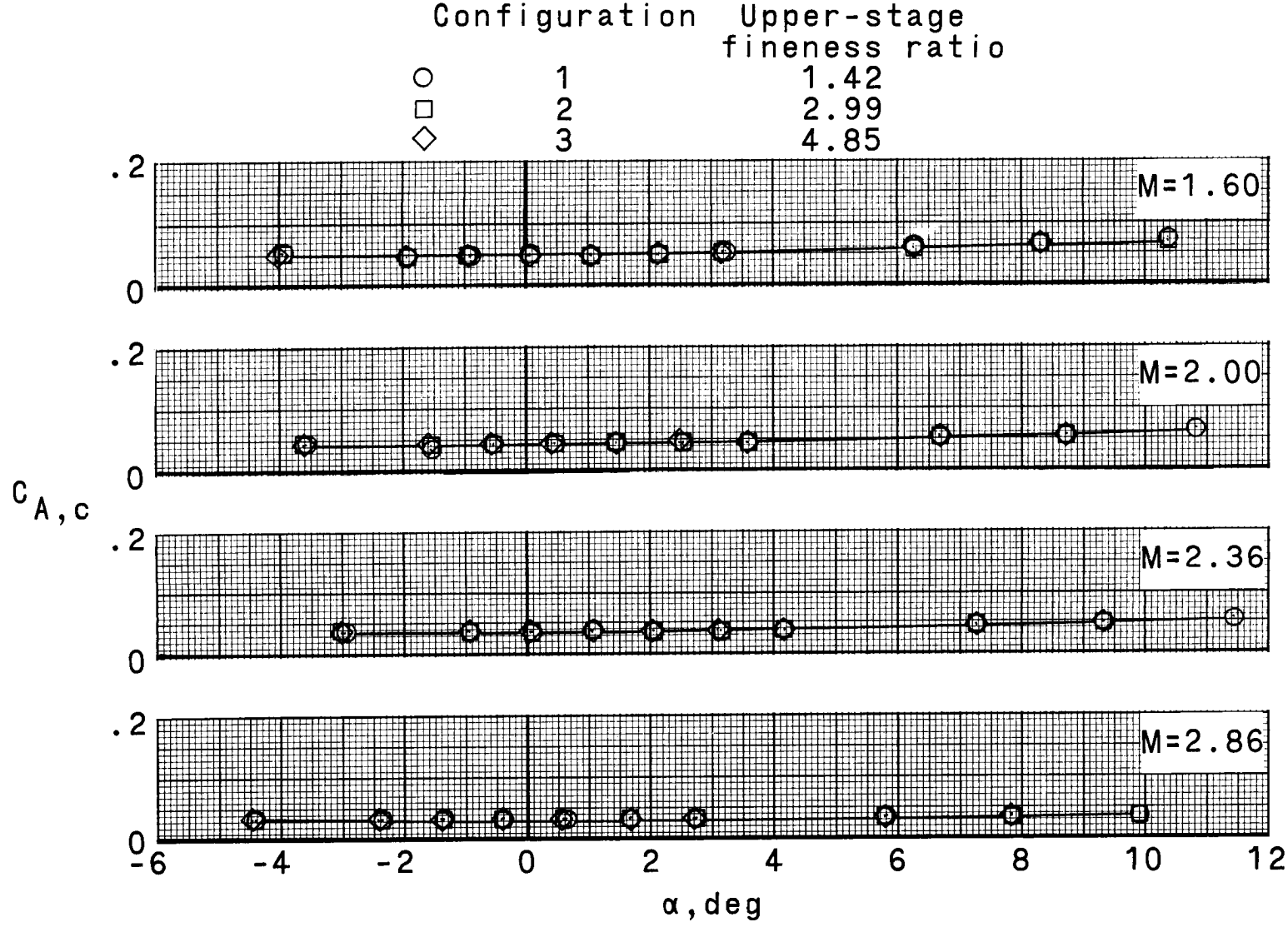


(b) Upper-stage fineness-ratio variation.

Figure 5.- Continued.

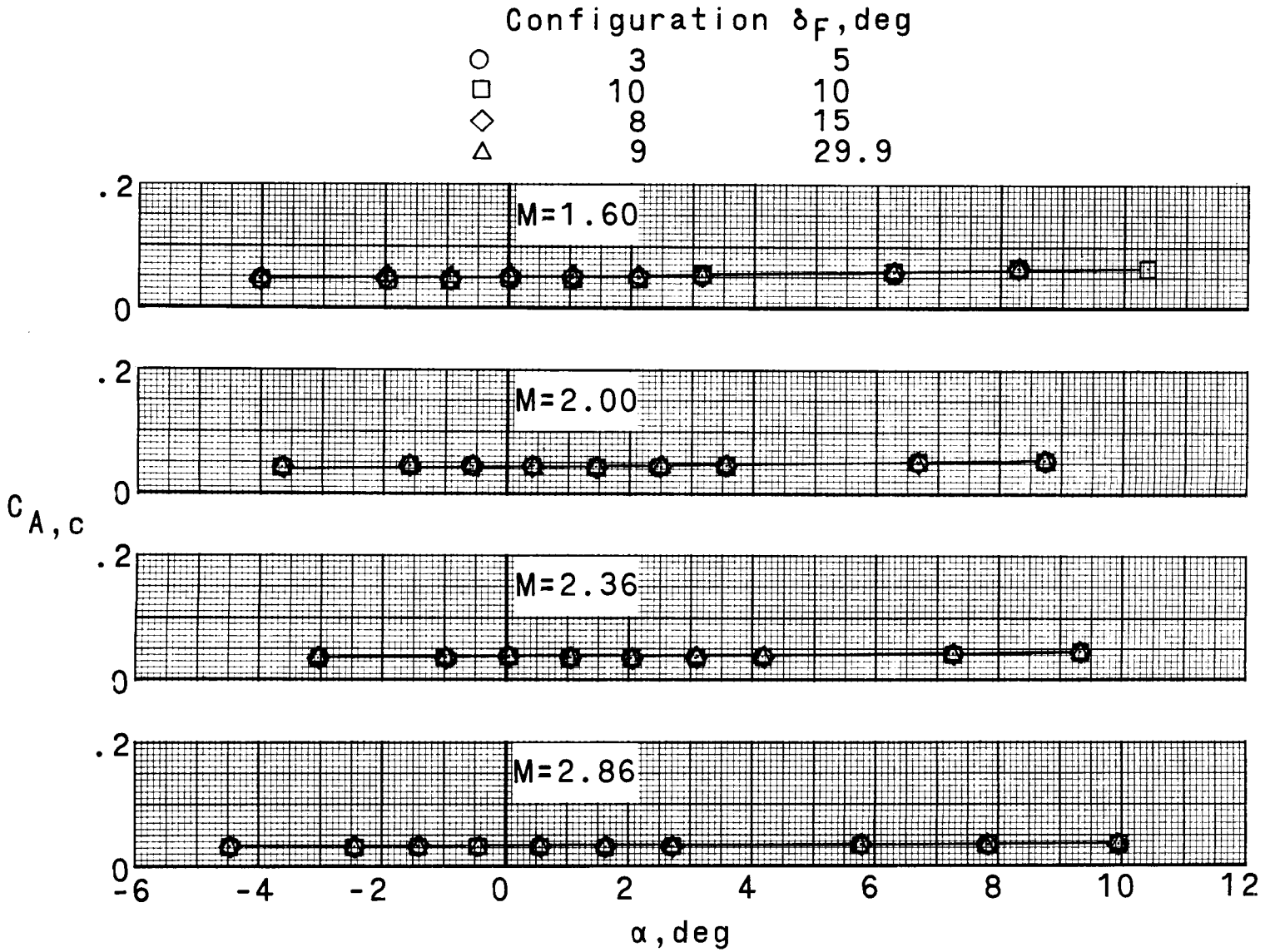


(c) Transition-flare-angle variation.

Figure 5.- Concluded.

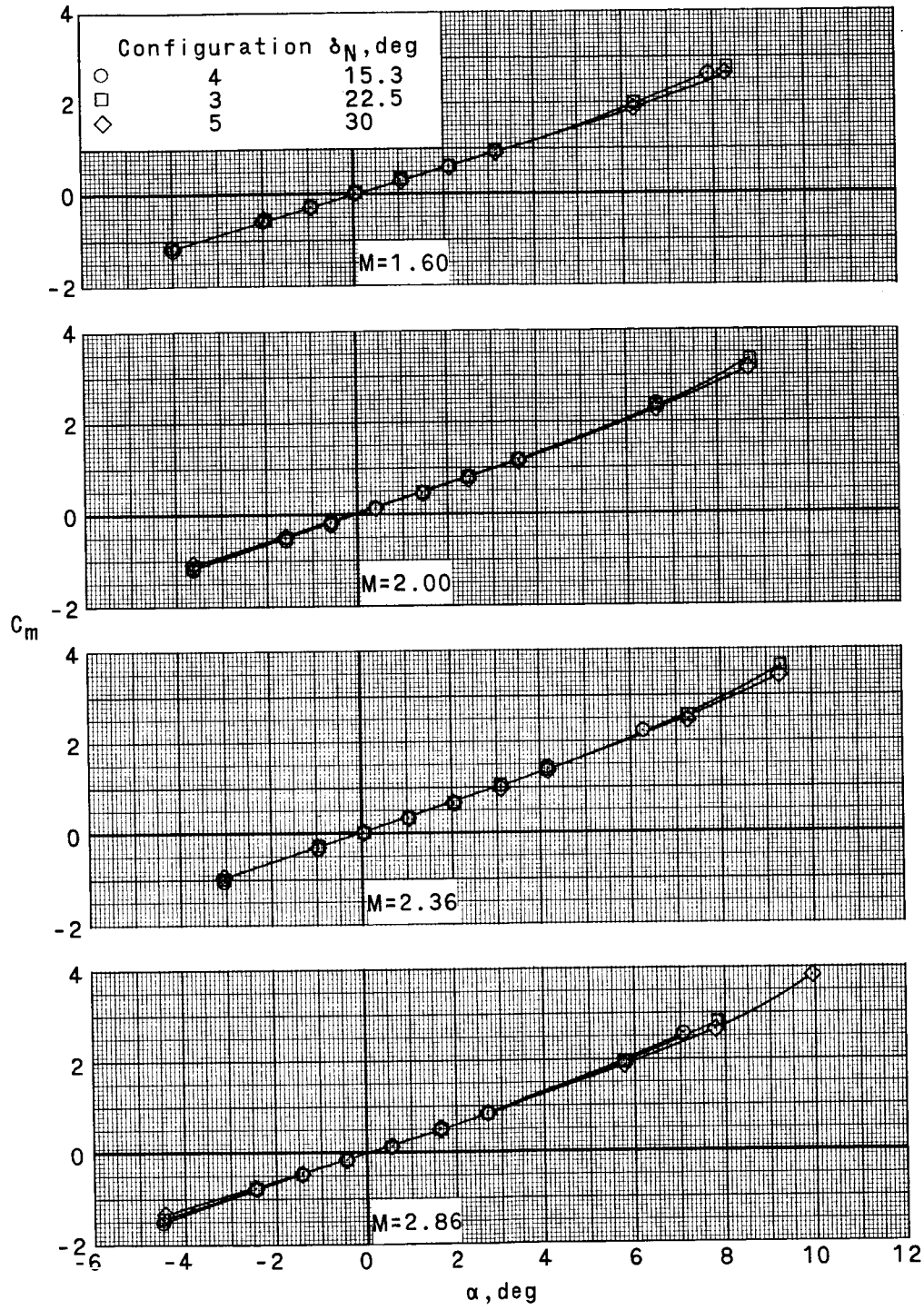


(a) Nose-cone-angle variations.

Figure 6.- Variation with angle of attack of pitching-moment characteristics.

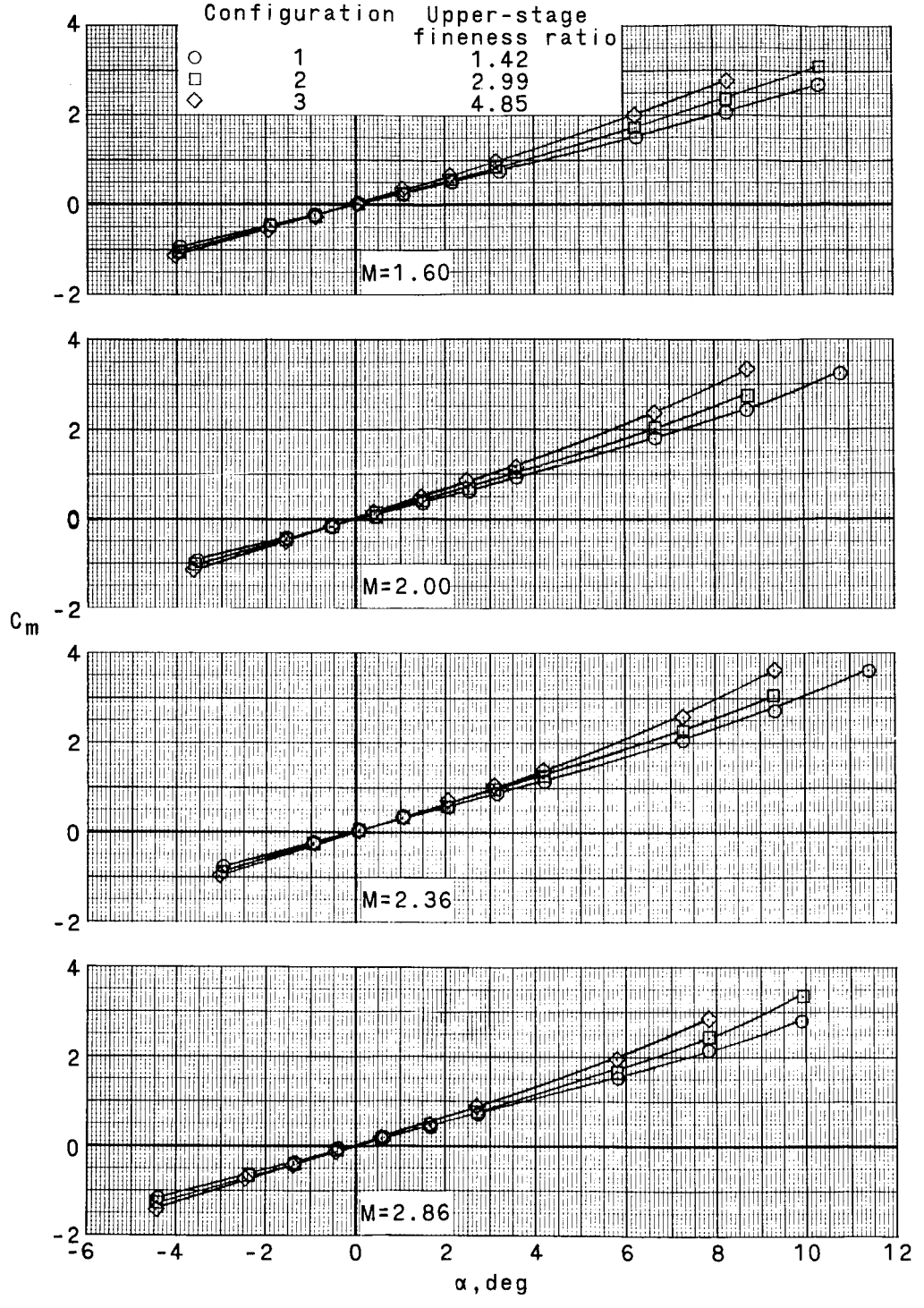


(b) Upper-stage fineness-ratio variations.

Figure 6.- Continued.

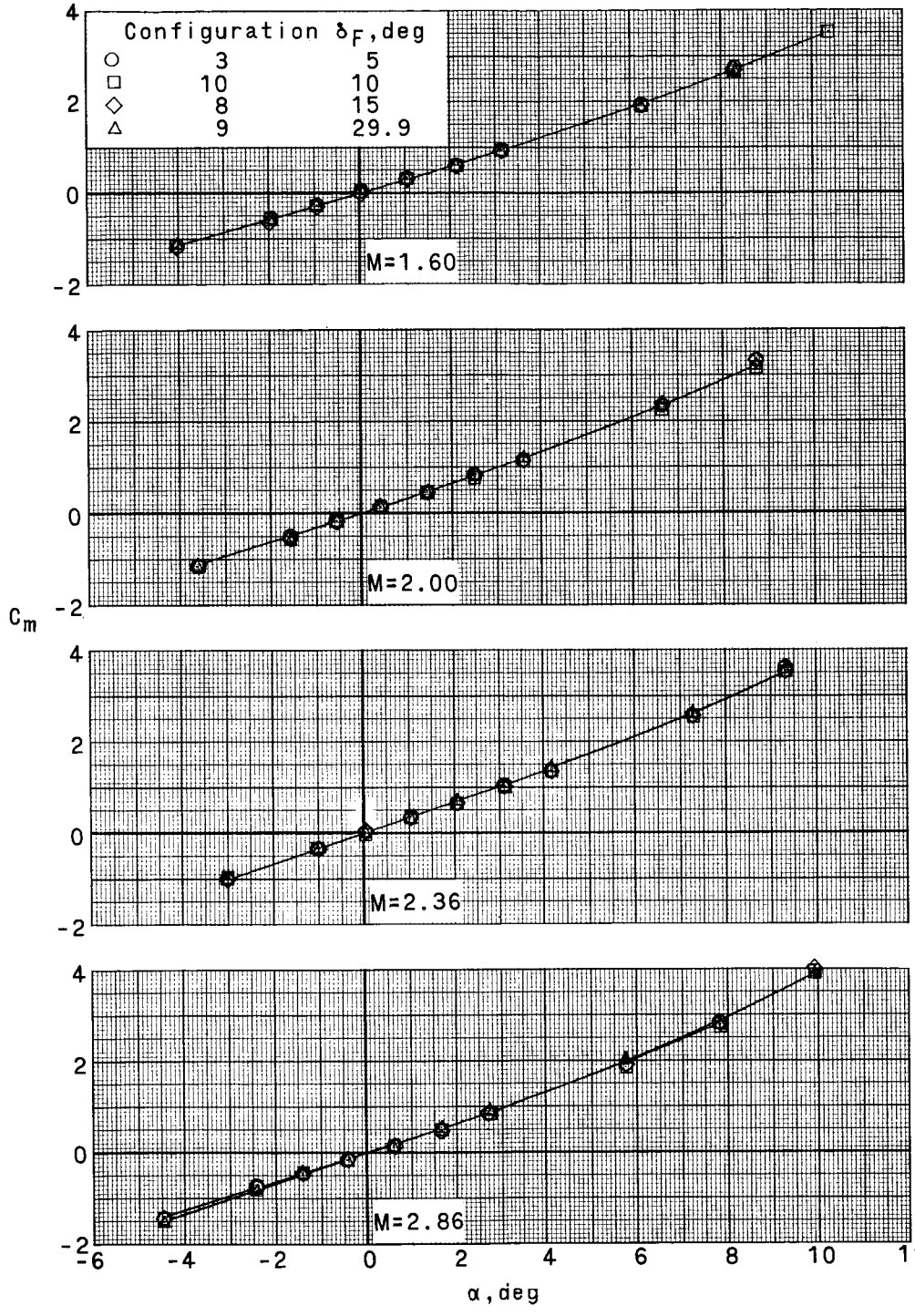


(c) Transition-flare-angle variations.

Figure 6.- Concluded.

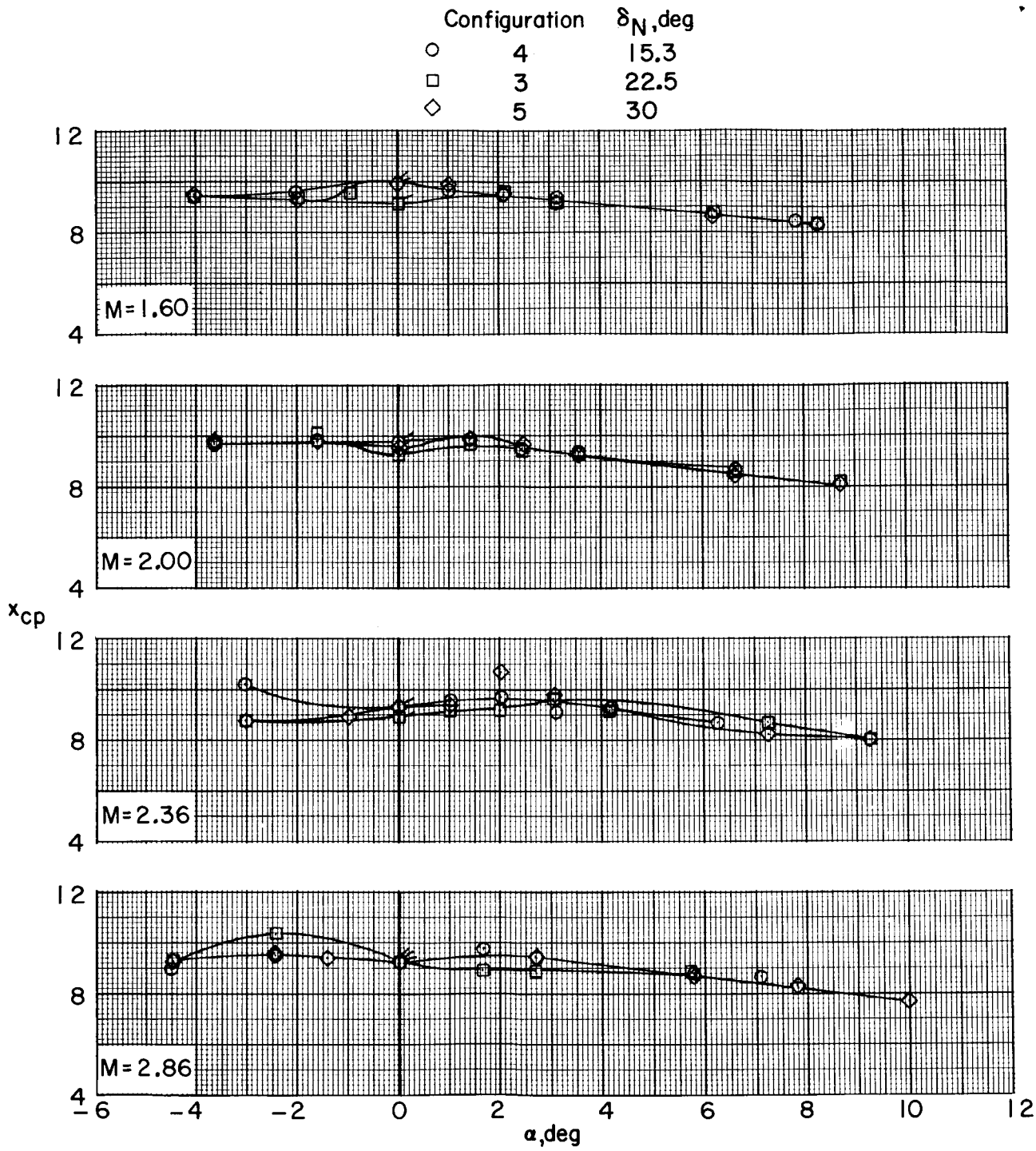


(a) Nose-cone-angle variations.

Figure 7.- Variation with angle of attack of center-of-pressure characteristics. (Flagged symbols indicate values obtained by using $C_{m_\alpha}$ and $C_{N_\alpha}$ measured at $\alpha \approx 0^\circ$.)

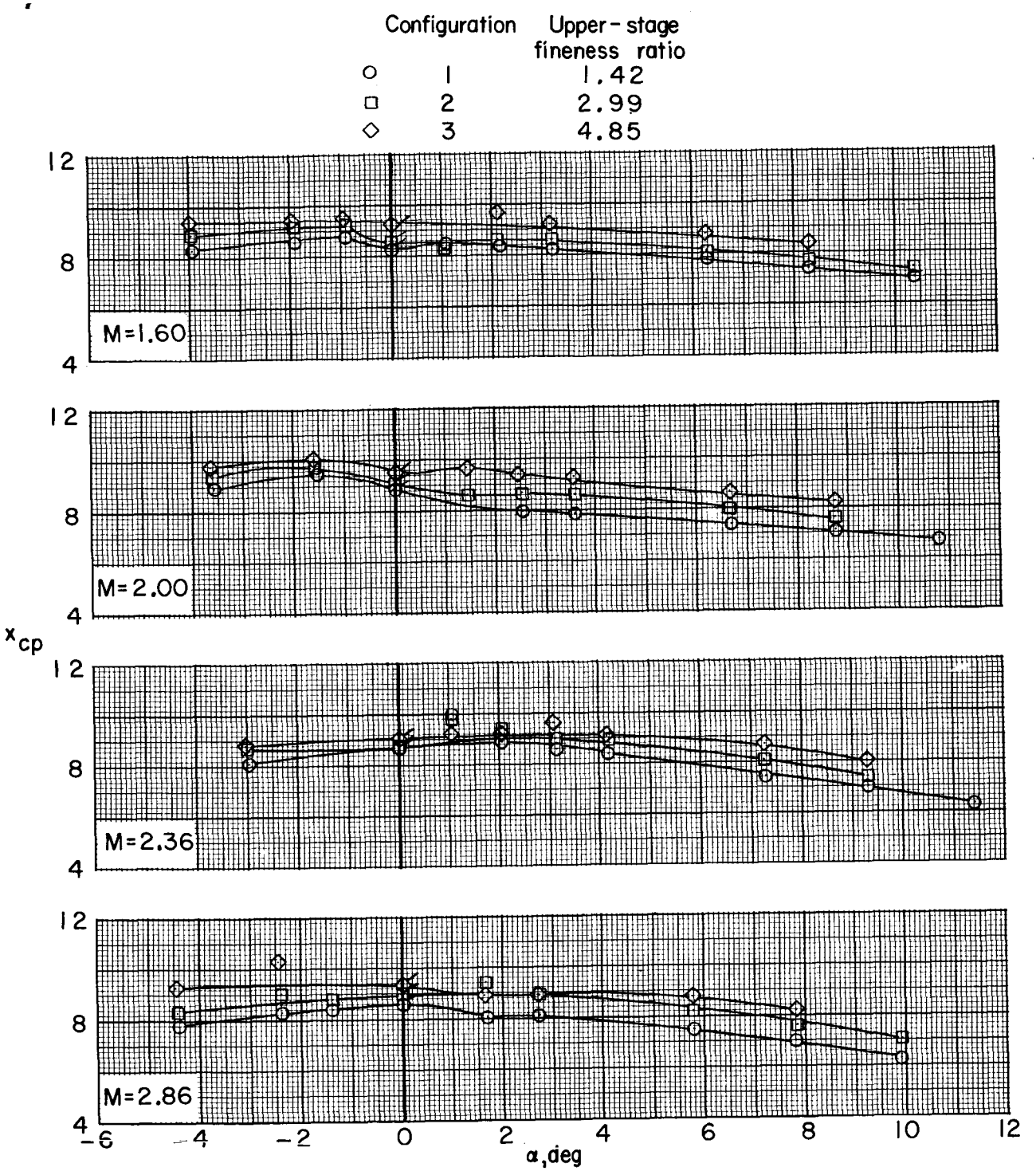


(b) Upper-stage fineness-ratio variations.

Figure 7.- Continued.

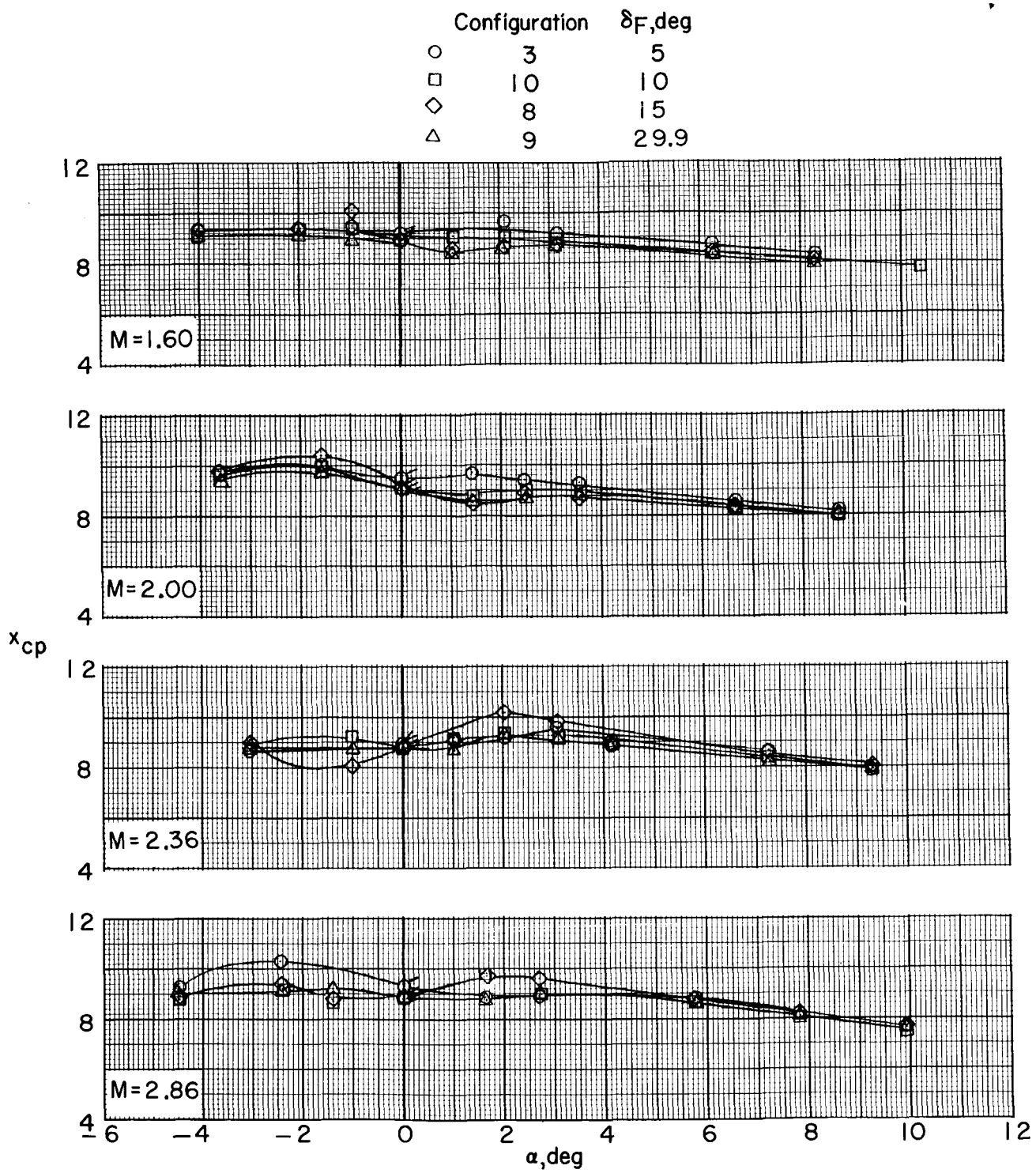


(c) Transition-flare-angle variations.

Figure 7.- Concluded.

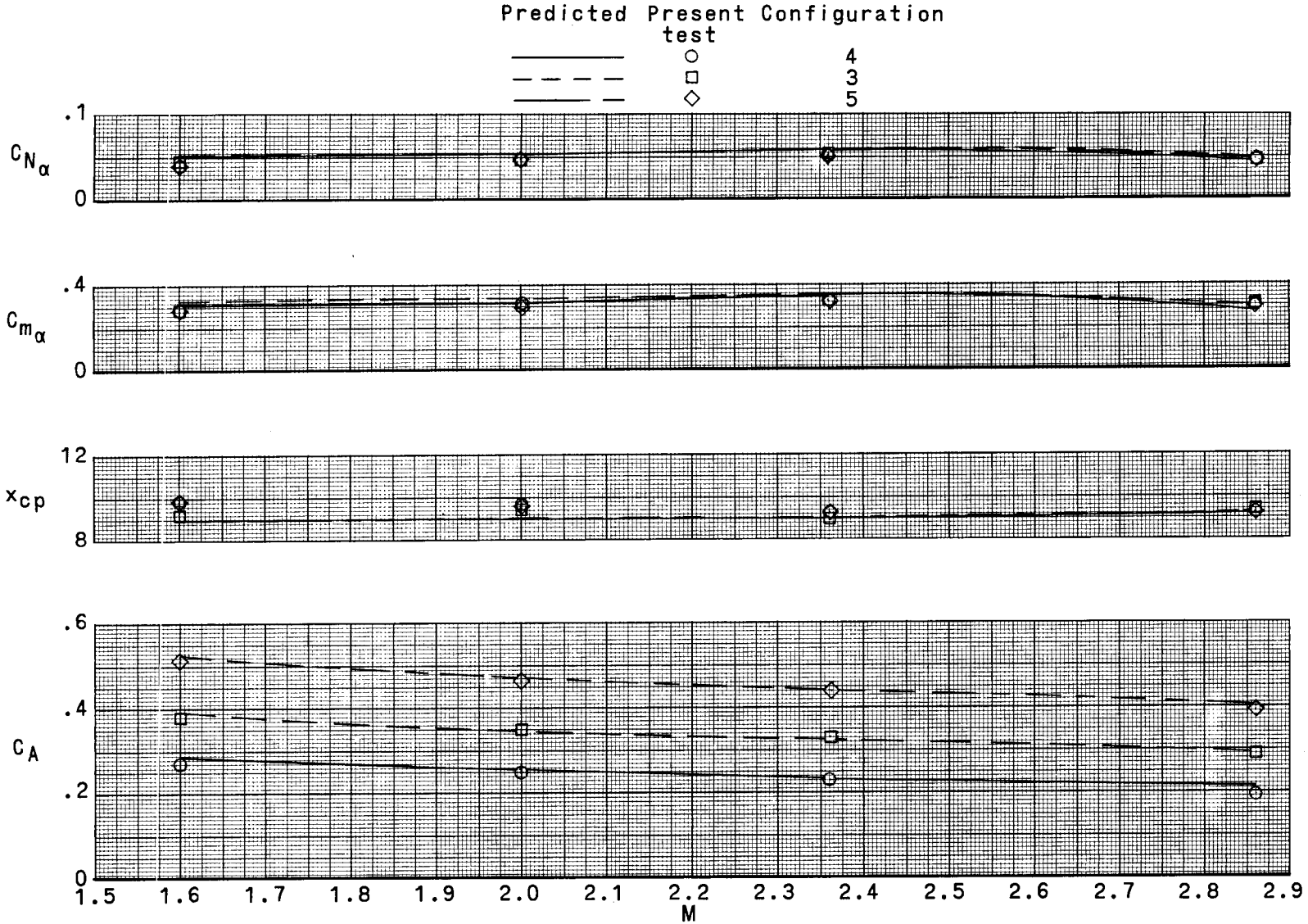


(a) Effect of nose-cone-angle variations.

Figure 8.- Summary of aerodynamic characteristics in pitch. $\alpha \approx 0^0$.

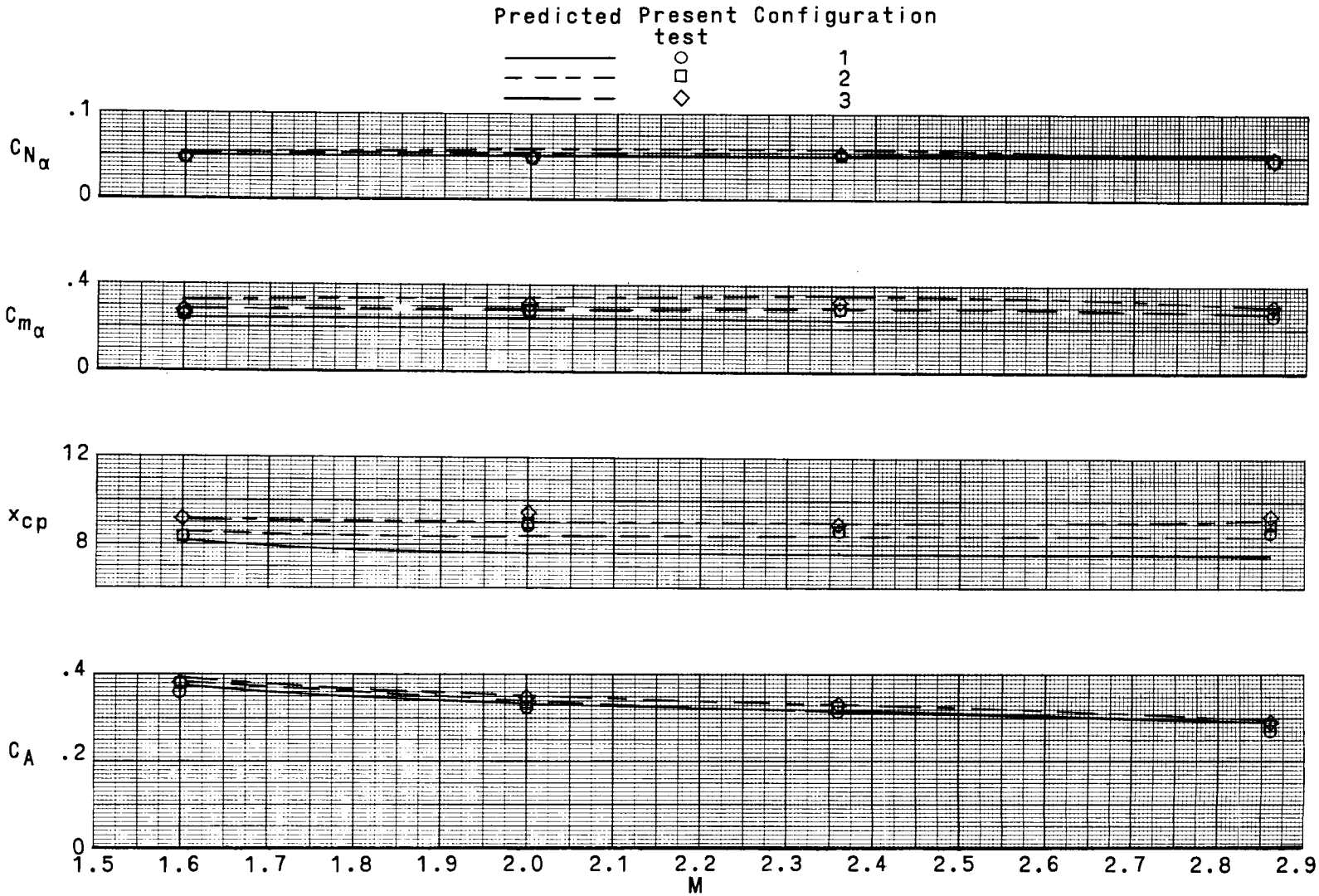


(b) Effect of upper-stage fineness-ratio variations.

Figure 8.- Continued.

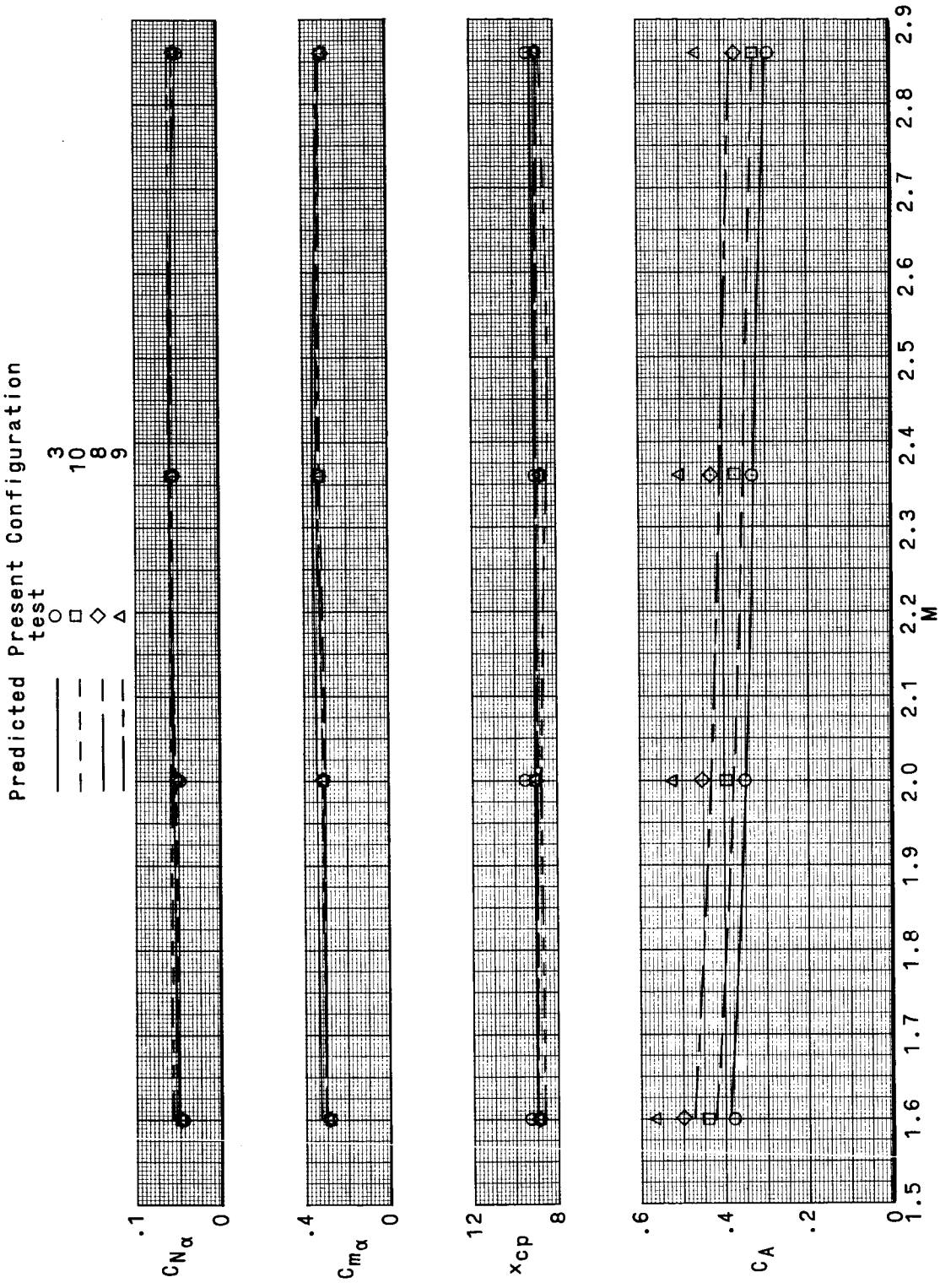


(c) Effect of transition-flare-angle variations.

Figure 8.- Concluded.

00464
1 cy
26-1-67

*"The aeronautical and space activities of the United States shall be conducted so as to contribute . . . to the expansion of human knowledge of phenomena in the atmosphere and space. The Administration shall provide for the widest practicable and appropriate dissemination of information concerning its activities and the results thereof."*

—NATIONAL AERONAUTICS AND SPACE ACT OF 1958

# NASA SCIENTIFIC AND TECHNICAL PUBLICATIONS

TECHNICAL REPORTS: Scientific and technical information considered important, complete, and a lasting contribution to existing knowledge.

TECHNICAL NOTES: Information less broad in scope but nevertheless of importance as a contribution to existing knowledge.

TECHNICAL MEMORANDUMS: Information receiving limited distribution because of preliminary data, security classification, or other reasons.

CONTRACTOR REPORTS: Technical information generated in connection with a NASA contract or grant and released under NASA auspices.

TECHNICAL TRANSLATIONS: Information published in a foreign language considered to merit NASA distribution in English.

TECHNICAL REPRINTS: Information derived from NASA activities and initially published in the form of journal articles.

SPECIAL PUBLICATIONS: Information derived from or of value to NASA activities but not necessarily reporting the results of individual NASA-programmed scientific efforts. Publications include conference proceedings, monographs, data compilations, handbooks, sourcebooks, and special bibliographies.

***Details on the availability of these publications may be obtained from:***

SCIENTIFIC AND TECHNICAL INFORMATION DIVISION

NATIONAL AERONAUTICS AND SPACE ADMINISTRATION

Washington, D.C. 20546